Electronic Supplementary Material (ESI) for RSC Advances.

Supporting Information

Prenylated Benzoylphloroglucinols and from the Leaves of *Garcinia multiflora*

Wenwei Fu,[a,b] *Man Wu,*[a,b] *Lunlun Zhu*[a,b], *Yuanzhi Lao*[a,b], *Liping Wang*[a,b], *Hongsheng Tan*[a,b], *Qinghong Yuan*[c] *and Hongxi Xu**[a,b]

[a] School of Pharmacy, Shanghai University of Traditional Chinese Medicine, Cai Lun Lu 1200, Shanghai 201203, People's Republic of China

[b] Engineering Research Center of Shanghai Colleges for TCM New Drug Discovery, Shanghai, People's Republic of China

[c] Department of Physics, East China Normal University, Dongchuan Road 500, Shanghai 200241, People's Republic of China

* To whom correspondence should be addressed. Fax: +86-21-51323089; Tel: +86-21-51323089; E-mail: xuhongxi88@gmail.com.

List of Supporting Information

Figure S60. HSQC NMR spectrum (CD_3OD, 600 MH_Z, 151 MH_Z) of GF-ox1

Figure S61. HMBC NMR spectrum (CD_3OD, 600 MH_Z, 150 MH_Z) of GF-ox1

Supporting Information Available

Part 1 Experimental section

Computational details

The theoretical calculations of compounds 1-3 was performed using Gaussian 09.[1] Conformational analysis was initially carried out using Maestro in Schrödinger 2010 conformational searching, together with the OPLS_2005 molecular mechanics methods. The optimized conformation geometries and thermodynamic parameters of all conformations were provided. The top twenty lowest energy conformers of the OPLS_2005 conformers were optimized further at B3LYP/6-31G (d, p) level. The minimum nature of the structure was confirmed by frequency calculations at the same computational level. The theoretical calculation of ECD was performed using time dependent Density Functional Theory (TDDFT) at B3LYP/6-31G (d, p) level in MeOH with PCM model. The calculated ECD curves were generated using SpecDis 1.62[2].

References:

(1) Gaussian 03, revision D.01, M. J. Frisch, G. W. Trucks, H. B. Schlegel, G. E. Scuseria, M. A. Robb, J. R. Cheeseman, J. J. A. Montgomery, T. Vreven, K. N. Kudin, J. C. Burant, J. M. Millam, S. S. Iyengar, J. Tomasi, V. Barone, B. Mennucci, M. Cossi, G. Scalmani, N. Rega, G. A. Petersson, H. Nakatsuji, M. Hada, M. Ehara, K. Toyota, R. Fukuda, J. Hasegawa, M. Ishida, T. Nakajima, Y. Honda, O. Kitao, H. Nakai, M. Klene, X. Li, J. E. Knox, H. P. Hratchian, J. B. Cross, V. Bakken, C. Adamo, J. Jaramillo, R. Gomperts, R. E. Stratmann, O. Yazyev, A. J. Austin, R. Cammi, C. Pomelli, J. W. Ochterski, P. Y. Ayala, K. Morokuma, G. A. Voth, P. Salvador, J. J. Dannenberg, V. G. Zakrzewski, S. Dapprich, A. D. Daniels, M. C. Strain, O.

Farkas, D. K. Malick, A. D. Rabuck, K. Raghavachari, J. B. Foresman, J. V. Ortiz, Q. Cui, A. G. Baboul, S. Clifford, J. Cioslowski, B. B. Stefanov, G. Liu, A. Liashenko, P. Piskorz, I. Komaromi, R. L. Martin, D. J. Fox, T. Keith, M. A. Al-Laham, C. Y. Peng, A. Nanayakkara, M. Challacombe, P. M. W. Gill, B. Johnson, W. Chen, M. W. Wong, C. Gonzalez, J. A. Pople, Gaussian, Inc., Wallingford CT, 2004.

(2) T. Bruhn, A. Schaumlöffel, Y. Hemberger, G. Bringmann, SpecDis version 1.62, University of Wuerzburg, Germany, 2014.

Part 2 Results and HRESIMS, ECD, IR, and NMR spectra of compounds 1–6.

1. Table S1. Cytotoxic IC_{50} Values of Crude Extracts and Key Fractions against Cancer Cell Lines

Table S1. Cytotoxic IC_{50} Values of Crude Extracts and Key Fractions against Cancer Cell Lines [a]

Fraction	HeLa	SGC7901	TE1	HCT116	Capan 2	HL-7702
I	91.13±4.65	92.01±9.15	72.44±6.52	72.58±3.61	＞100	62.52±0.55
II	22.53±1.83	23.33±0.20	21.81±0.89	20.81±0.94	36.91±0.75	27.16±2.33
III	＞100	＞100	＞100	＞100	＞100	＞100
IV	＞100	＞100	＞100	＞100	＞100	＞100
Paclitaxel	0.54±0.35	0.34±0.02	0.25±0.025	0.16±0.021	3.50±0.18	0.24±0.06

a. Results are expressed as mean IC_{50} values in μg/ml (Extracts) or μM (Paclitaxel). I: Extracts with acetone from the leaves of *G. multiflora*; II: Extracts from I on silica gel eluted by CH_2Cl_2; III: Extracts from I on silica gel eluted by CH_2Cl_2-MeOH (9:1, v/v); IV: Extracts from I on silica gel eluted by CH_2Cl_2-MeOH (1:1, v/v).

2. Figue CS1 Optimized geometries of predominant conformers for 1 (a–j)

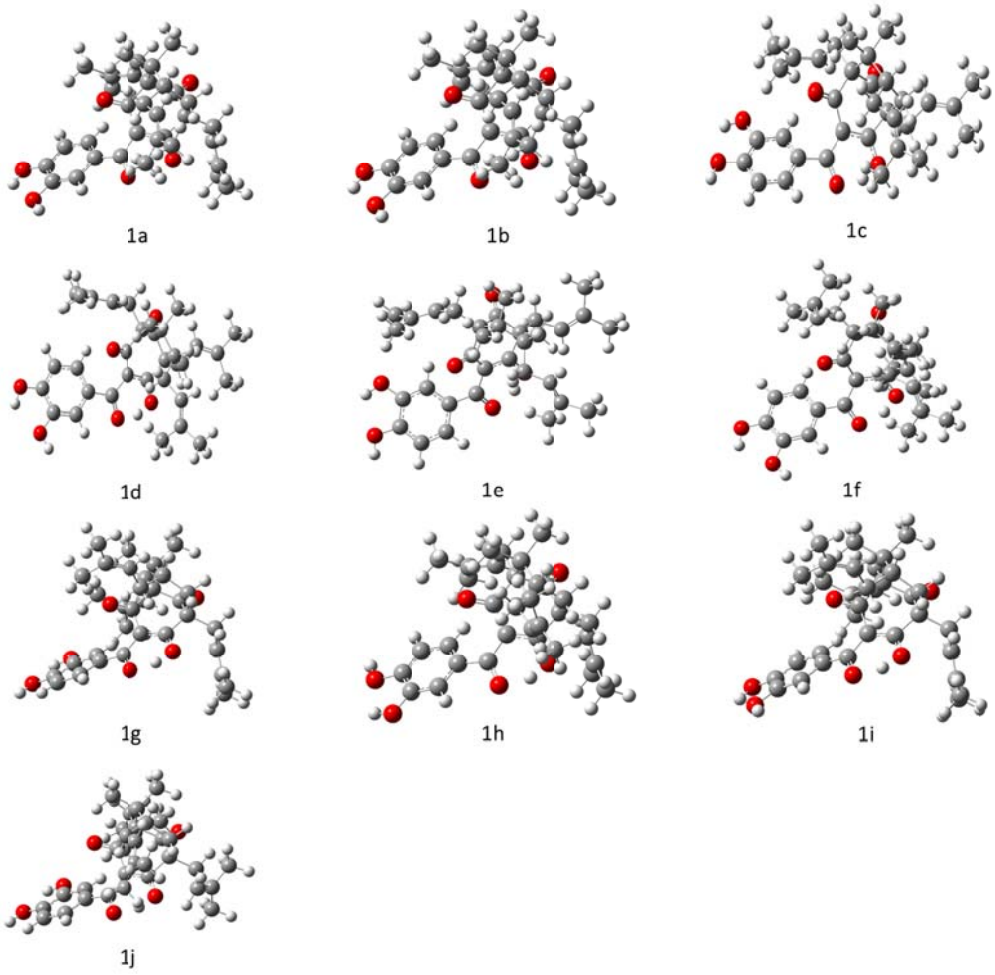

Optimized geometries of predominant conformers for **1** (**a**–**j**) at the B3LYP/6-31G (d, p) level in MeOH with PCM model

3. Table CS1. Calculated Relative Energies (Kcal/mol) and Boltzmann distributions of the optimized 1 at B3LYP/6-31G (d, p) level in MeOH with PCM model.

Calculated Relative Energies (Kcal/mol) and Boltzmann distributions of the optimized **1** at B3LYP/6-31G (d, p) level in MeOH with PCM model .

Conformations	*G*	*Δ*E	%
1a	-1734.188528	0.00	46.17
1b	-1734.187682	0.53	18.83
1c	-1734.187238	0.81	11.76
1d	-1734.186488	1.28	5.31
1e	-1734.186236	1.44	4.06
1f	-1734.186121	1.51	3.60
1g	-1734.185879	1.66	2.78
1h	-1734.185724	1.76	2.36
1i	-1734.185229	2.07	1.40
1j	-1734.185155	2.12	1.29

*Δ*E: Relative to 1a; %: Boltzmann distributions, using the relative Gibbs free energies as weighting factors

4. Figure CS2. Optimized geometries of predominant conformers for 2 (a–j) at the B3LYP/6-31G (d, p) level in MeOH with PCM model

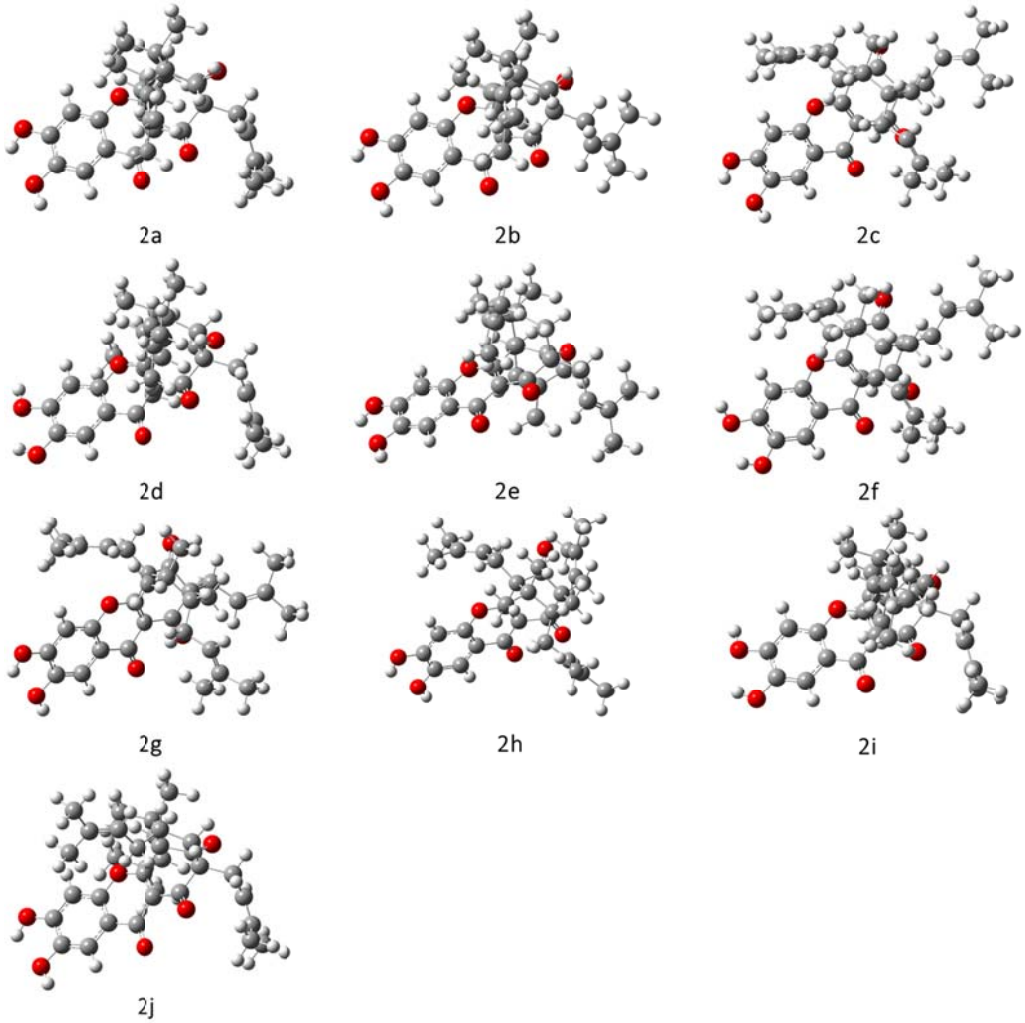

Optimized geometries of predominant conformers for **2** (**a**–**j**) at the B3LYP/6-31G (d, p) level in MeOH with PCM model

5. Table CS2. Calculated Relative Energies (Kcal/mol) and Boltzmann distributions of the optimized 2 at B3LYP/6-31G (d, p) level in MeOH with PCM model.

Calculated Relative Energies (Kcal/mol) and Boltzmann distributions of the optimized **2** at B3LYP/6-31G (d, p) level in MeOH with PCM model.

Conformations	G	*ΔE*	%
2a	-1732.975785	0.00	30.42
2b	-1732.975286	0.31	17.91
2c	-1732.975037	0.47	13.77
2d	-1732.974819	0.61	10.92
2e	-1732.974099	1.06	5.09

2f	-1732.974079	1.07	4.99
2g	-1732.974027	1.10	4.72
2h	-1732.973836	1.22	3.85
2i	-1732.973595	1.37	2.98
2j	-1732.97296	1.77	1.52

⊿E: Relative to 1a; %: Boltzmann distributions, using the relative Gibbs free energies as weighting factors

6. **Figure CS3. Optimized geometries of predominant conformers for 3 (a–h) at the B3LYP/6-31G (d, p) level in MeOH with PCM model**

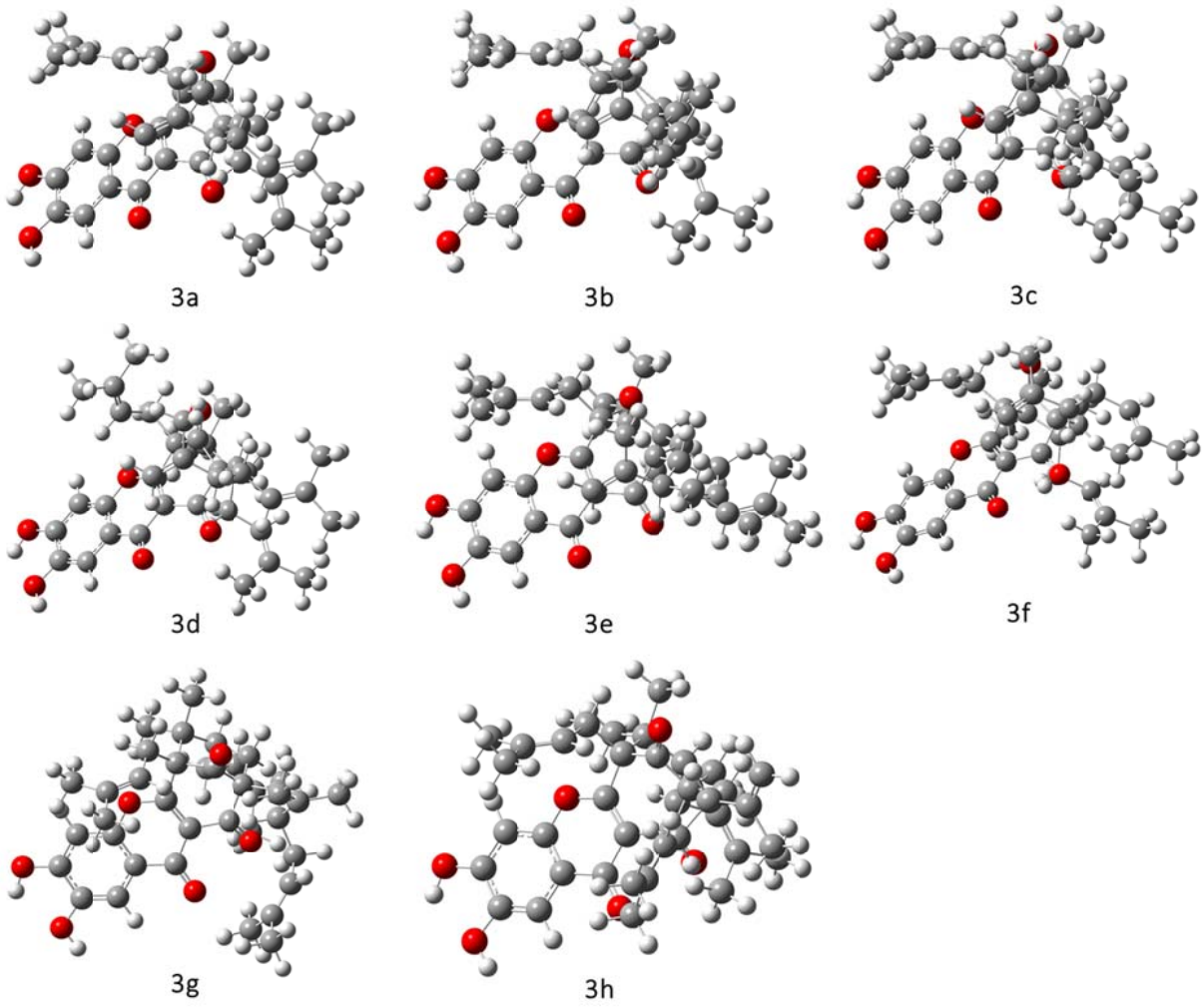

Optimized geometries of predominant conformers for **3** (**a**–**h**) at the B3LYP/6-31G (d, p) level in MeOH with PCM model

7. **Table CS3.** Calculated Relative Energies (Kcal/mol) and Boltzmann distributions of the optimized **3** at B3LYP/6-31G (d, p) level in MeOH with PCM model

Calculated Relative Energies (Kcal/mol) and Boltzmann distributions of the optimized **3** at B3LYP/6-31G (d, p) level in MeOH with PCM model.

Conformations	G	*ΔE*	%
3a	-1928.319848	0.00	28.65
3b	-1928.319661	0.12	23.5
3c	-1928.319265	0.37	15.44
3d	-1928.31881	0.65	9.53
3e	-1928.318669	0.74	8.21
3f	-1928.318572	0.80	7.41
3g	-1928.317915	1.21	3.69
3h	-1928.317733	1.33	3.04

*Δ*E: Relative to 1a; %: Boltzmann distributions, using the relative Gibbs free energies as weighting factors

Figure S1. HRESIMS spectrum of **1**

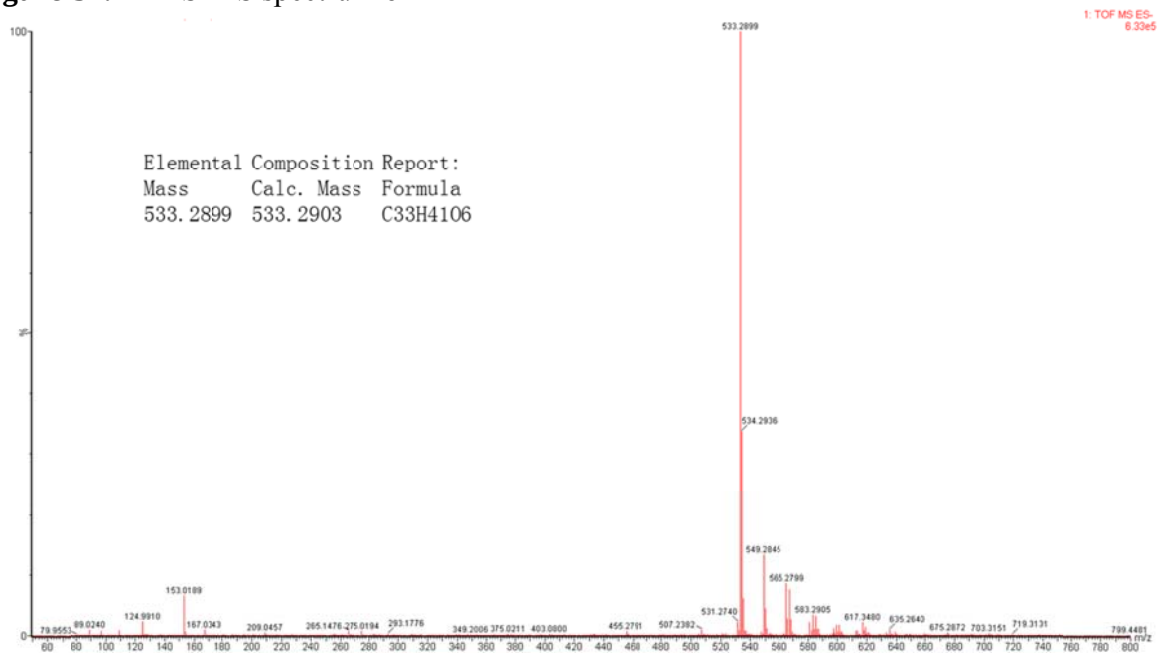

Figure S2. Experimental UV spectrum of **1**

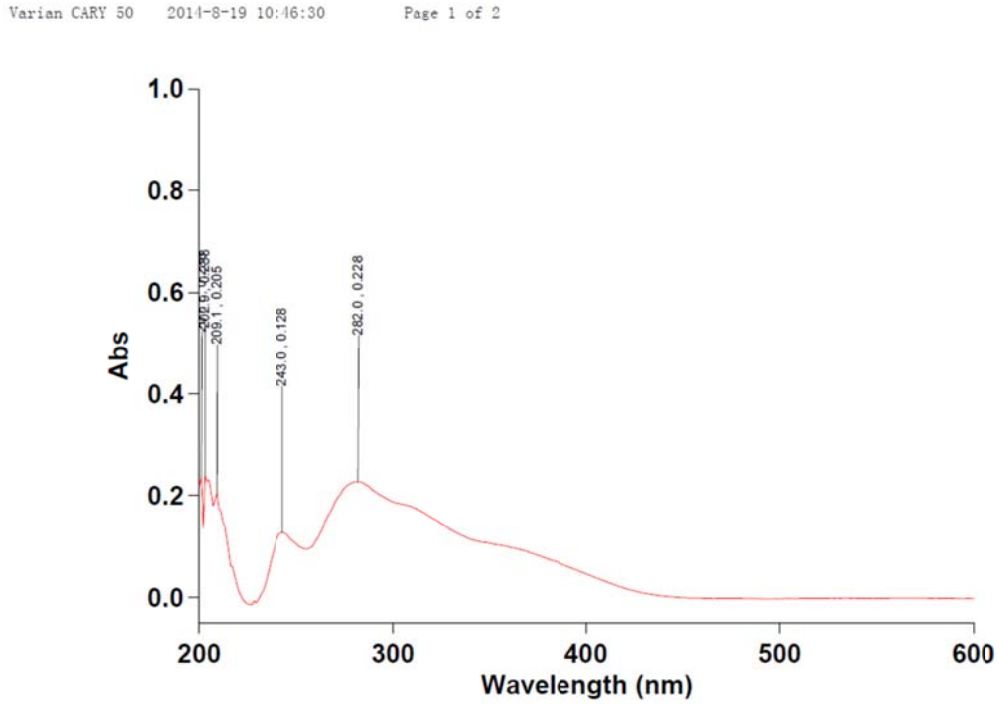

Figure S3. Experimental ECD spectrum of **1**

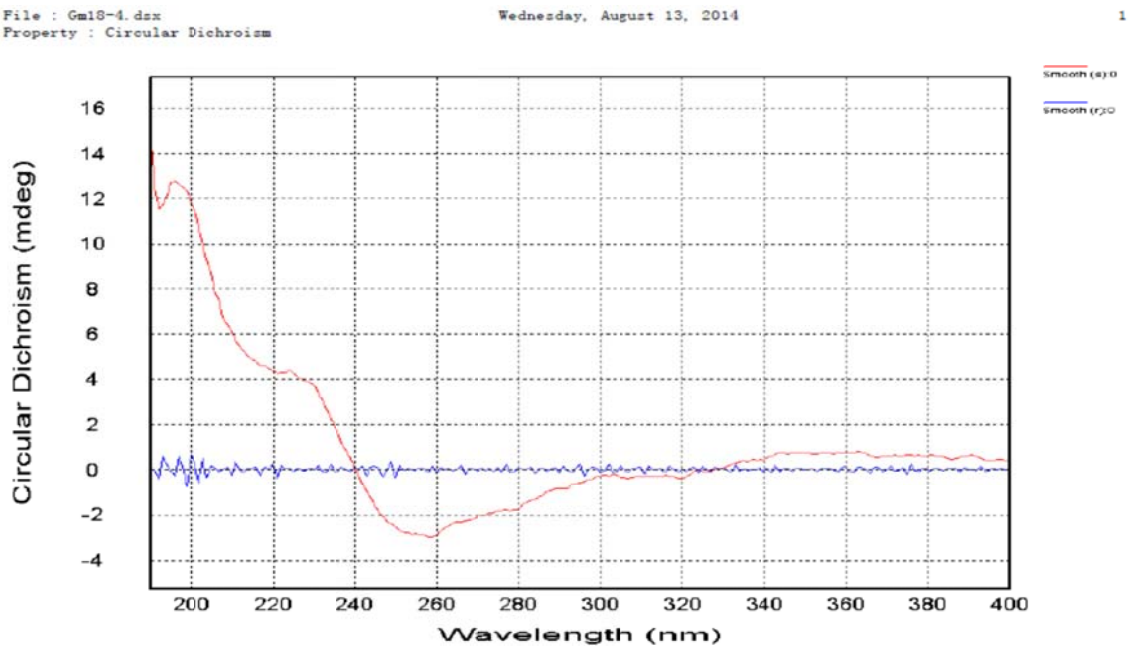

Figure S4. IR (KBr, disc) spectrum of **1**

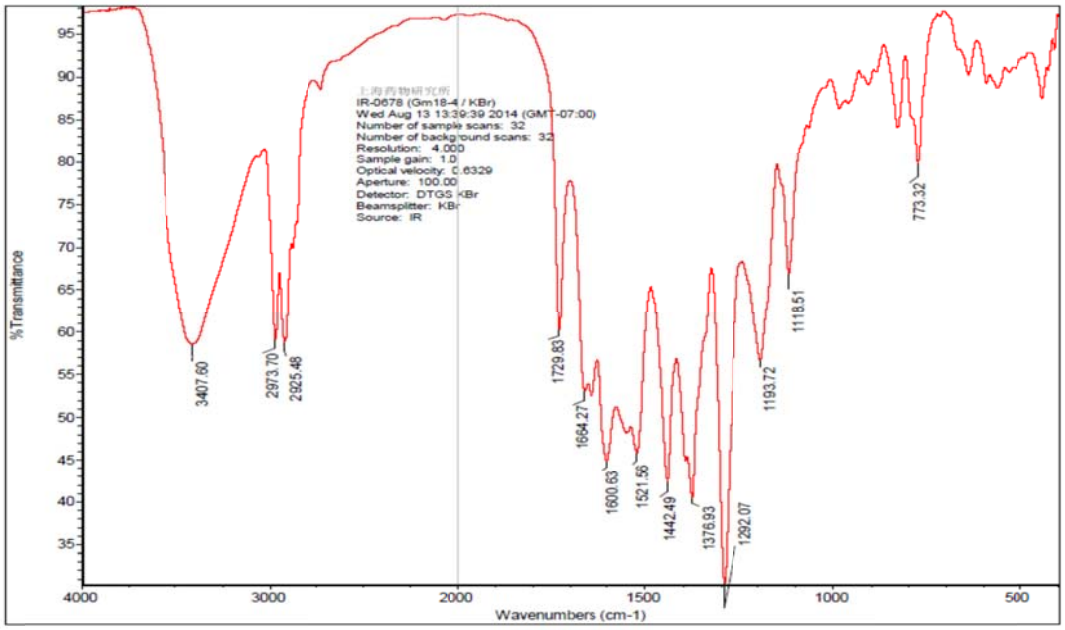

Figure S5. ^{1}H NMR spectrum (CD_3OD, 600 MH_Z) of **1**

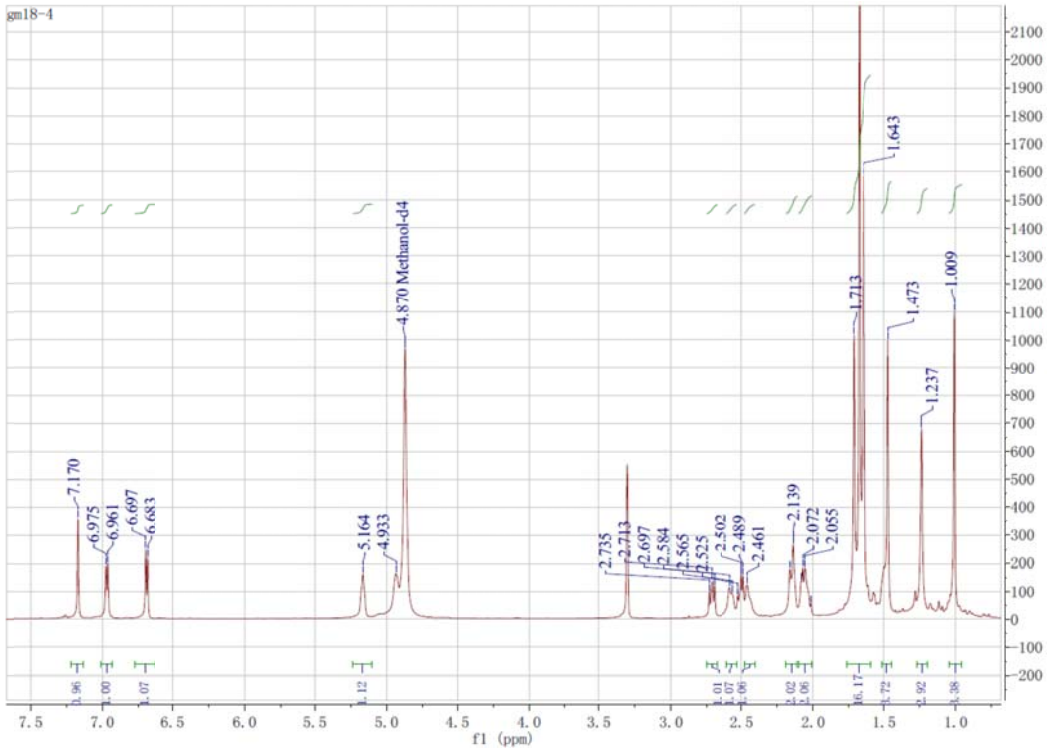

Figure S6. ^{13}C NMR spectrum (CD_3OD, 151 MH_Z) of **1**

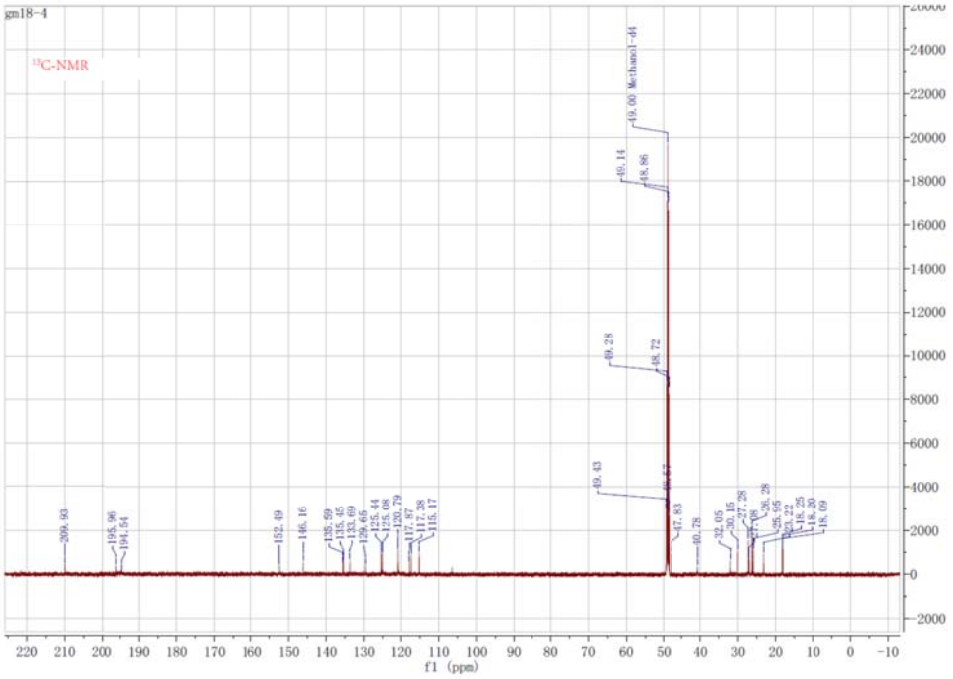

Figure S7. DEPT and ^{13}C NMR spectrum (CD_3OD, 151 MH_Z) of **1**

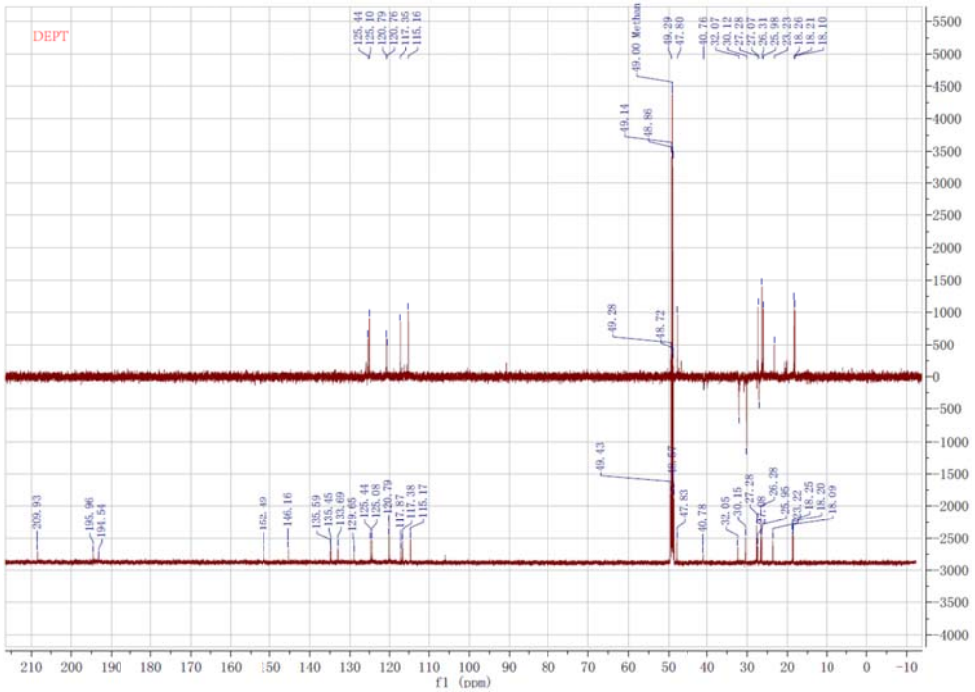

Figure S8. HSQC NMR spectrum (CD_3OD, 600 MH_Z, 151 MH_Z) of **1**

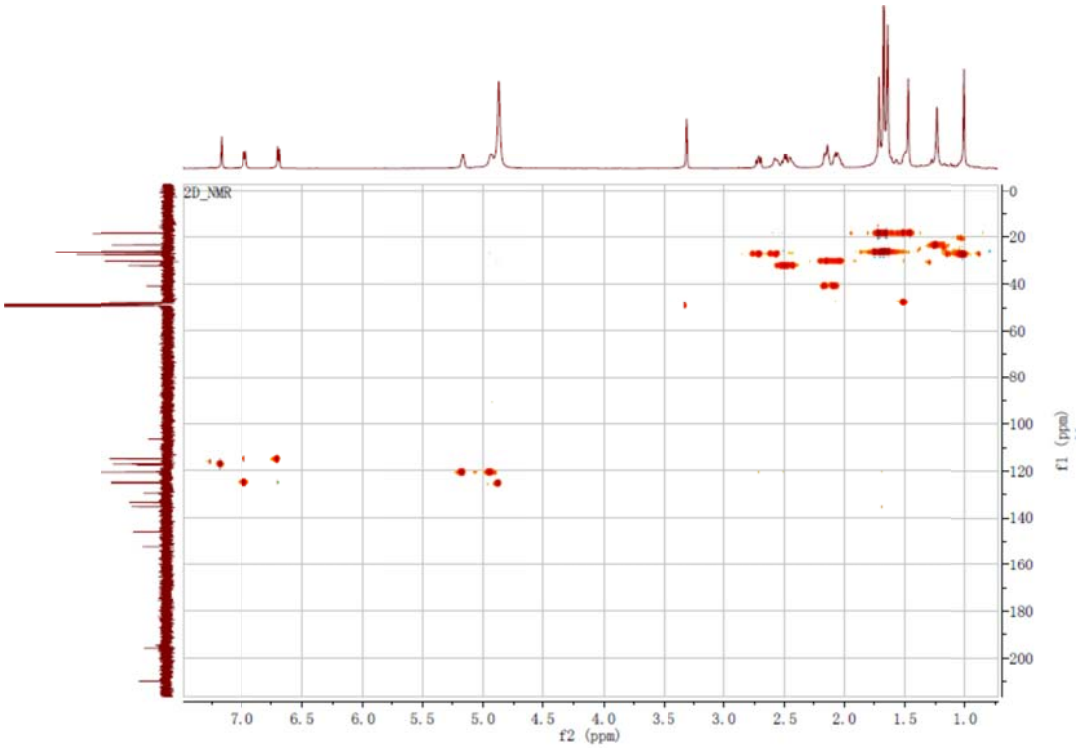

Figure S9. HMBC NMR spectrum (CD_3OD, 600 MH_Z, 151 MH_Z) of **1**

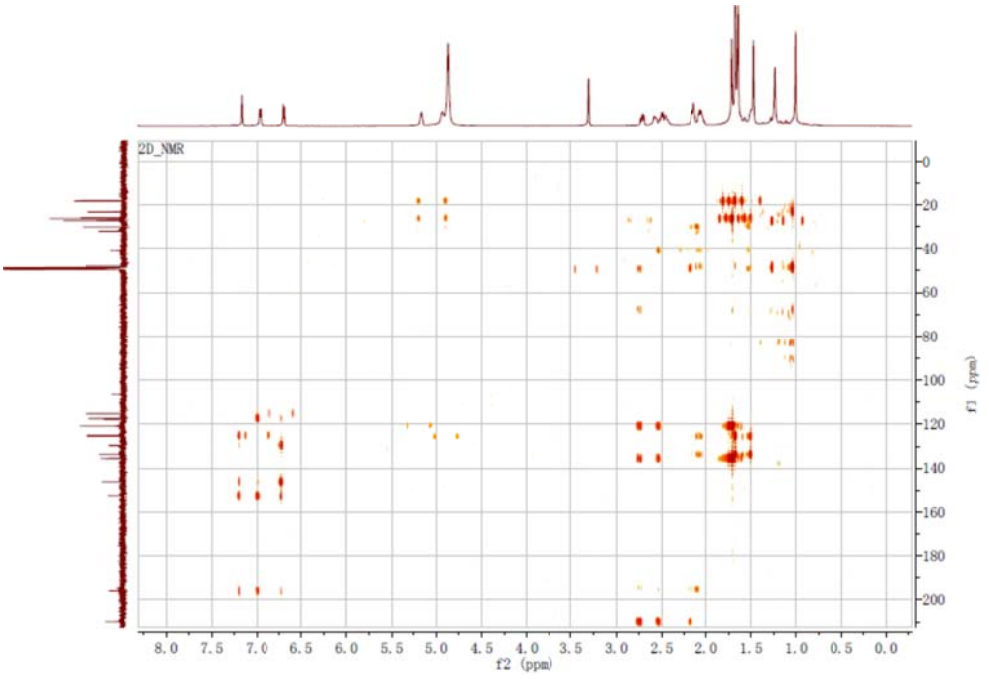

Figure S10. TOCSY NMR spectrum (CD_3OD, 600 MH_Z) of **1**

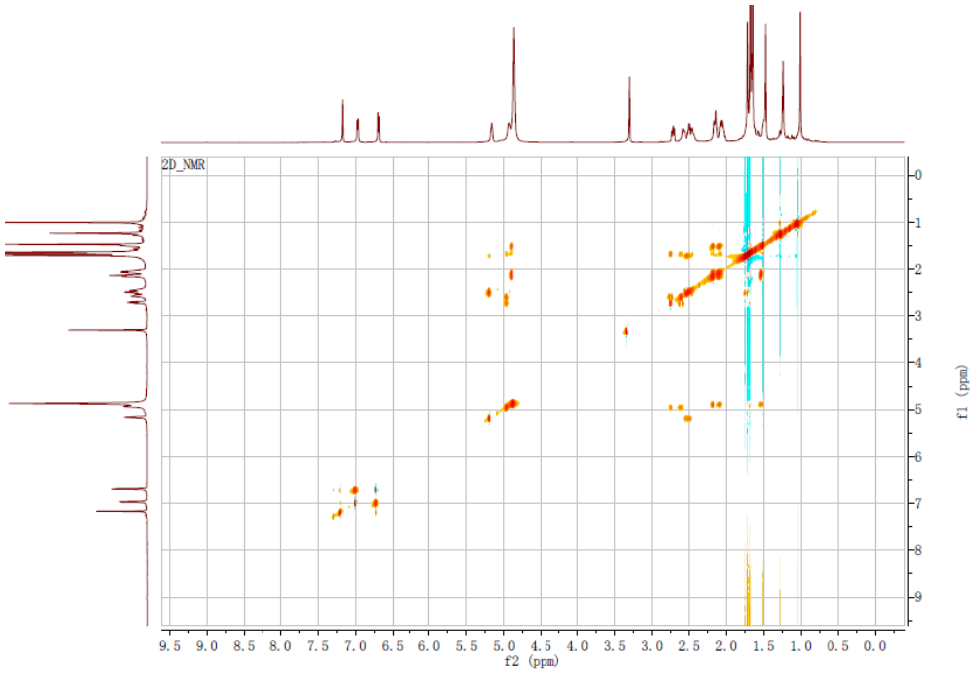

Figure S11. NOESY NMR spectrum (CD_3OD, 600 MH_Z) of **1**

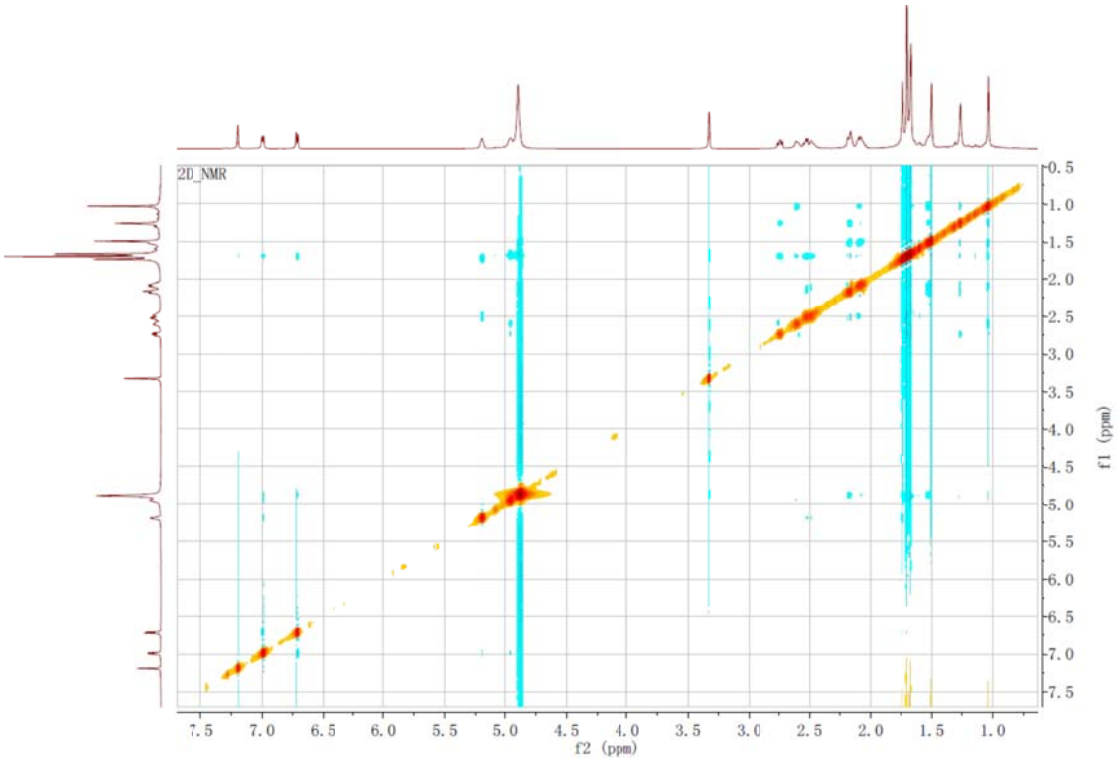

Figure S12. HRESIMS spectrum of **2**

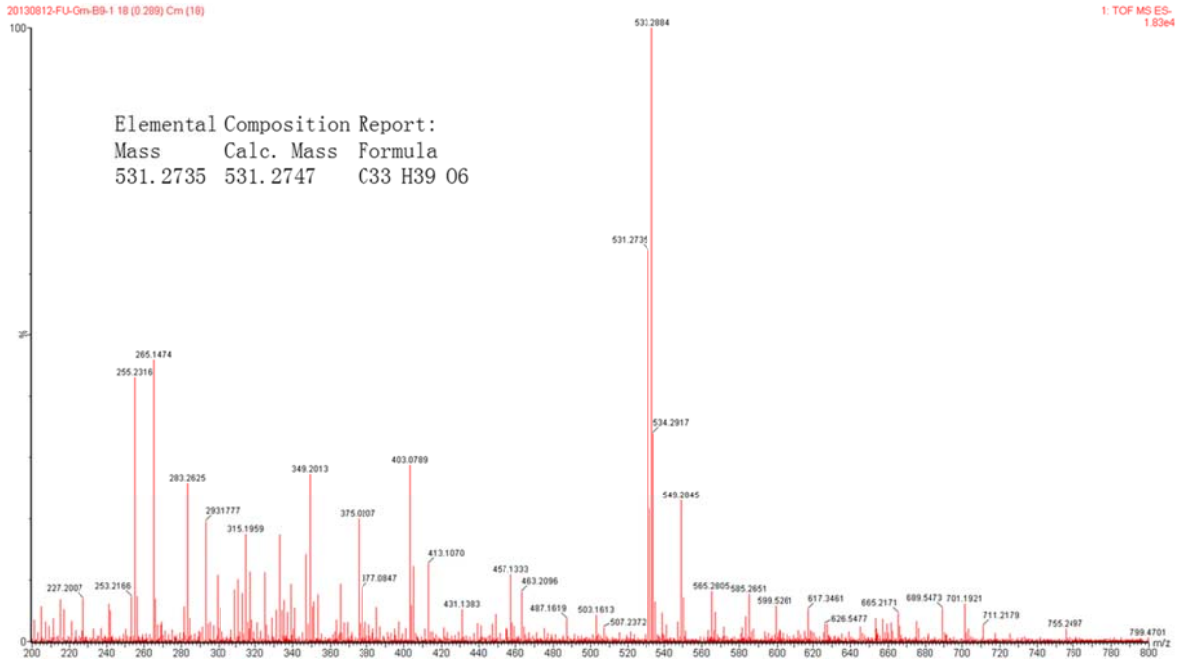

Figure S13. Experimental UV spectrum of **2**

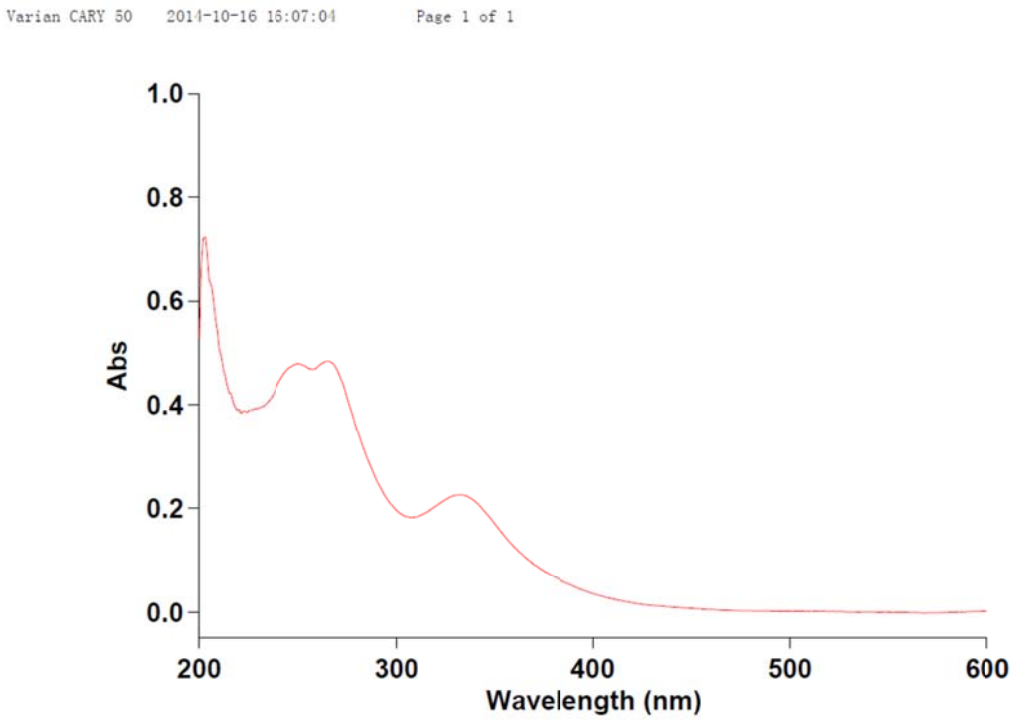

Figure S13. Experimental ECD spectrum of **2**

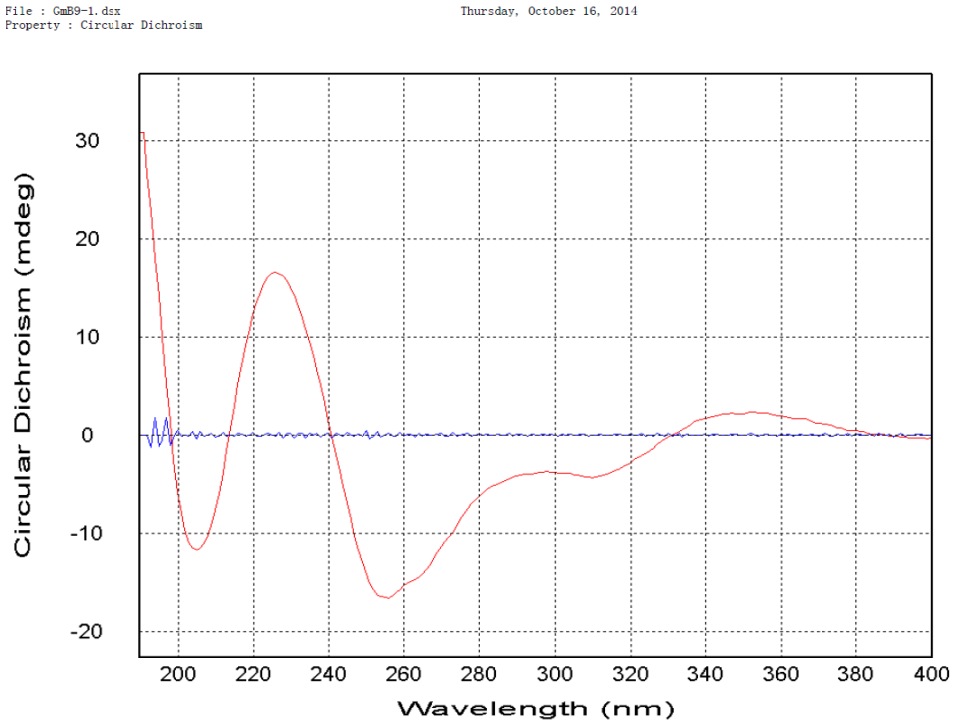

Figure S14. IR (KBr, disc) spectrum of **2**

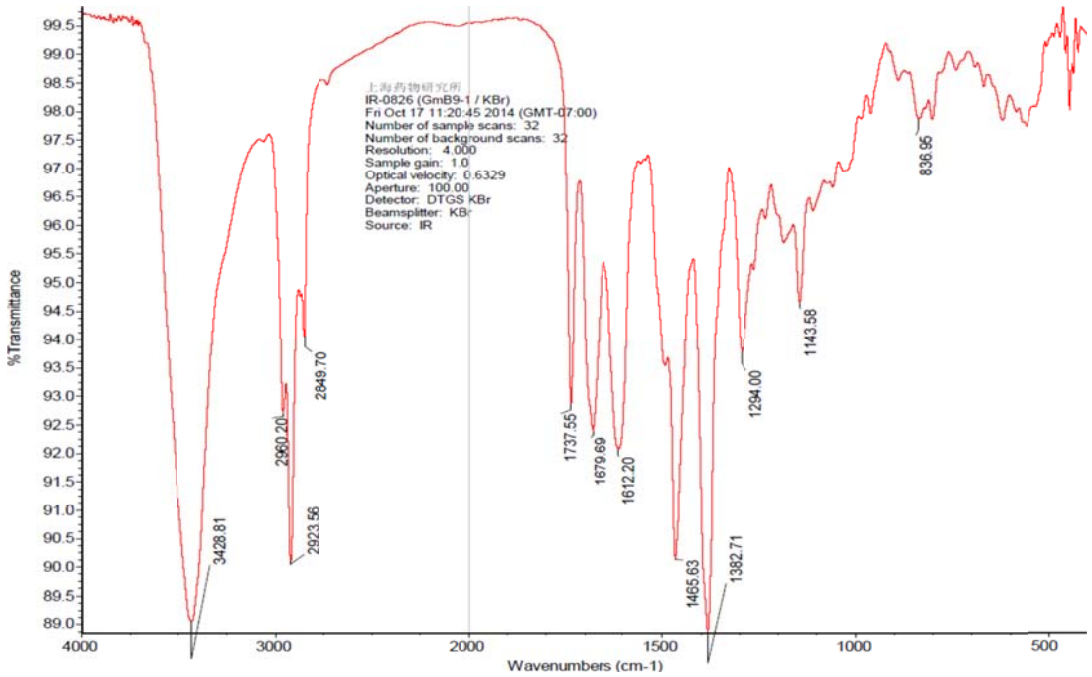

Figure S15. ^{1}H NMR spectrum (DMSO-d_6, 400 MHz) of **2**

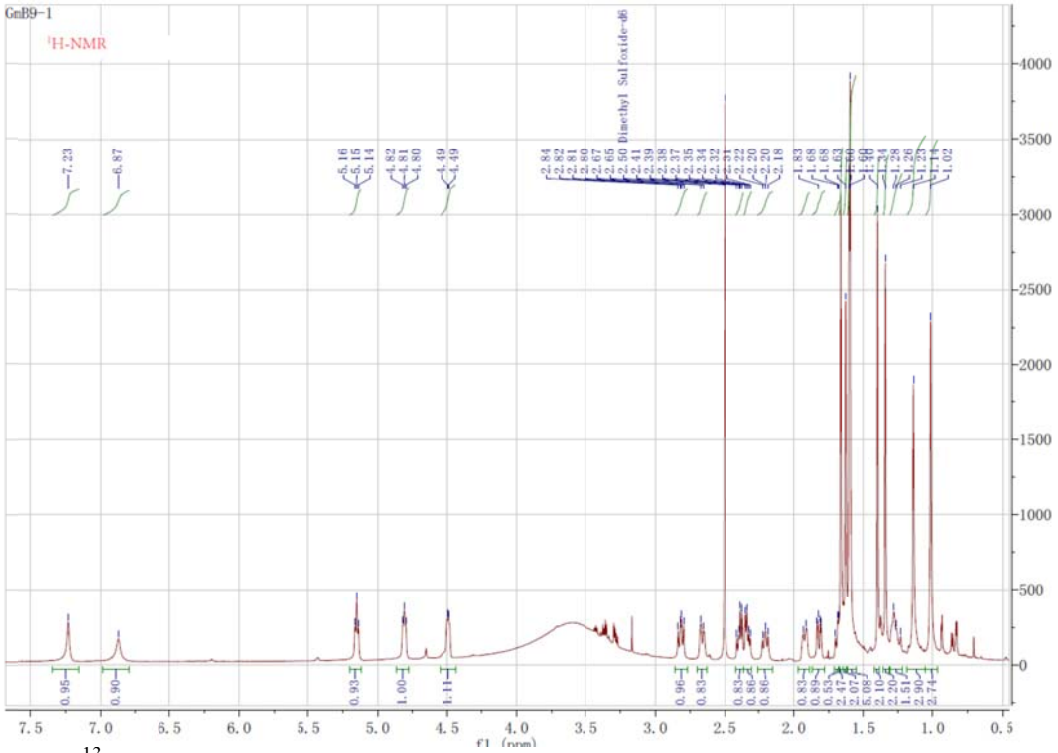

Figure S16. ^{13}C NMR spectrum (DMSO-d_6, 151 MHz) of **2**

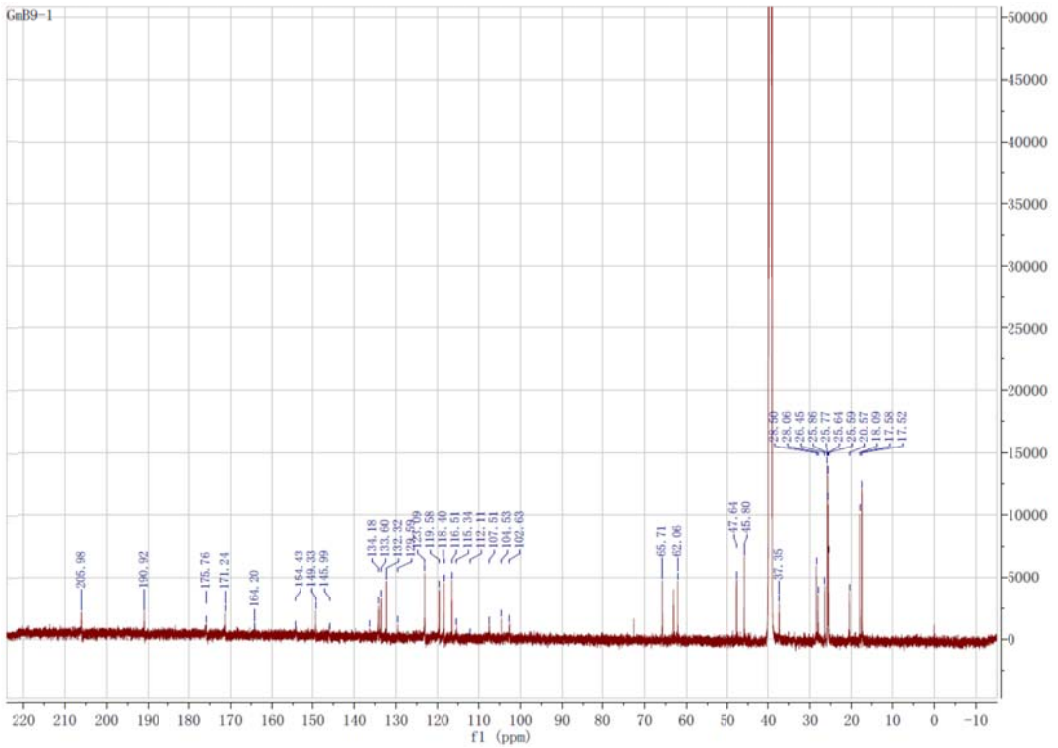

Figure S17. DEPT and ^{13}C-NMR spectrum (DMSO-d_6, 100 MHz) of **2**

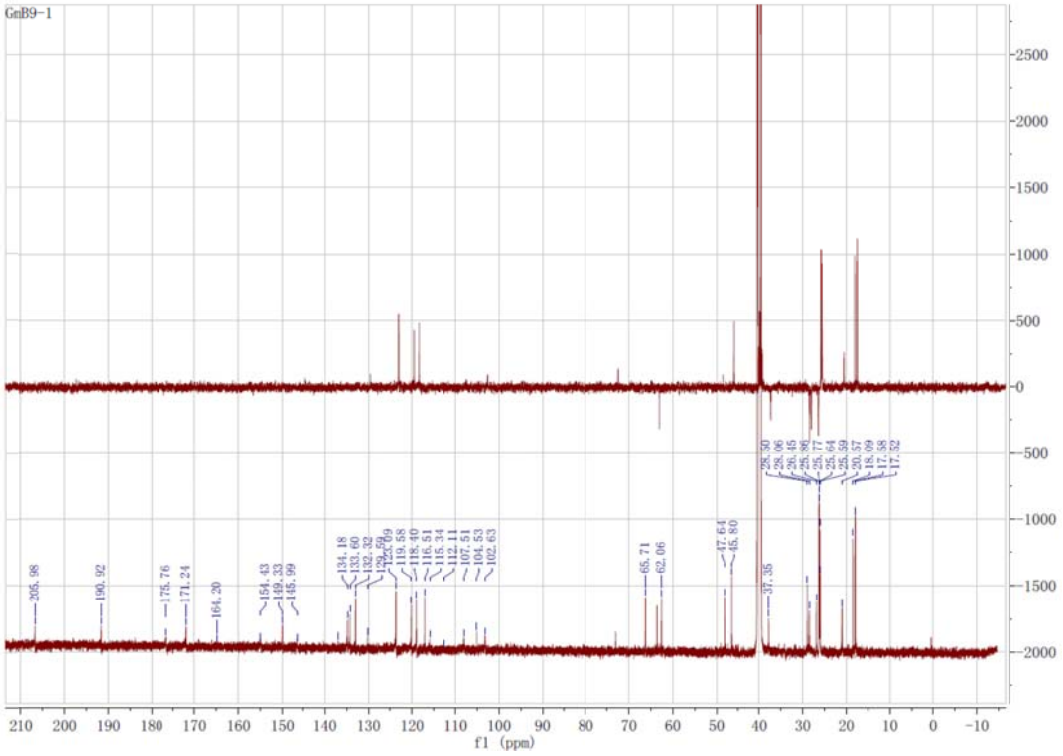

Figure S18. HSQC NMR spectrum (DMSO-d_6, 600 MHz, 151 MHz) of **2**

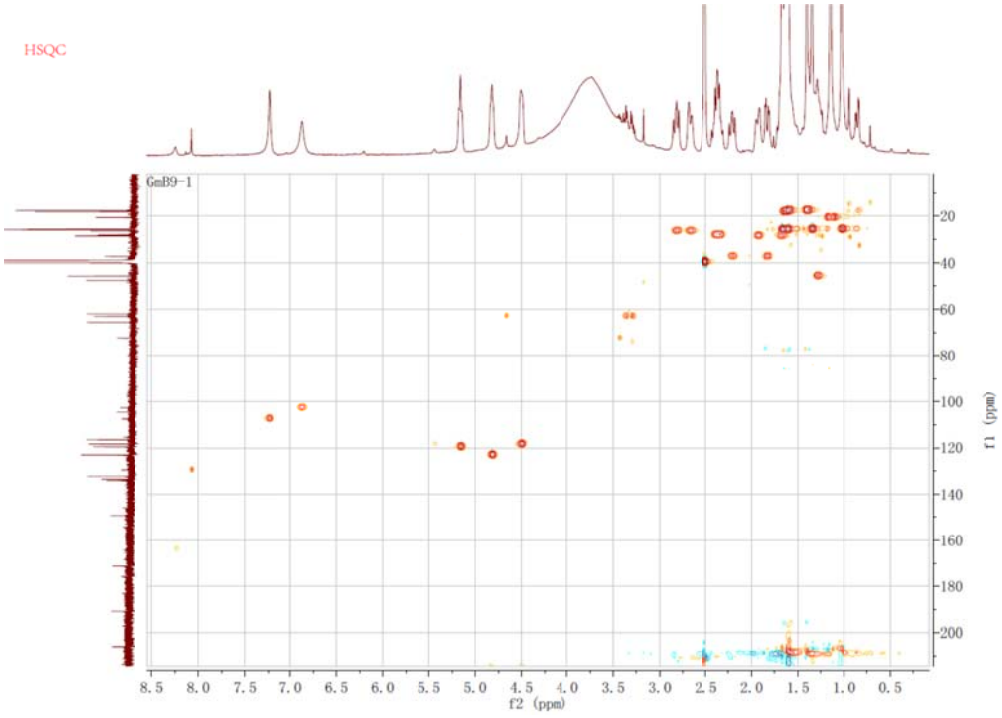

Figure S19. HMBC NMR spectrum (DMSO-d_6, 600 MHz, 151 MHz) of **2**

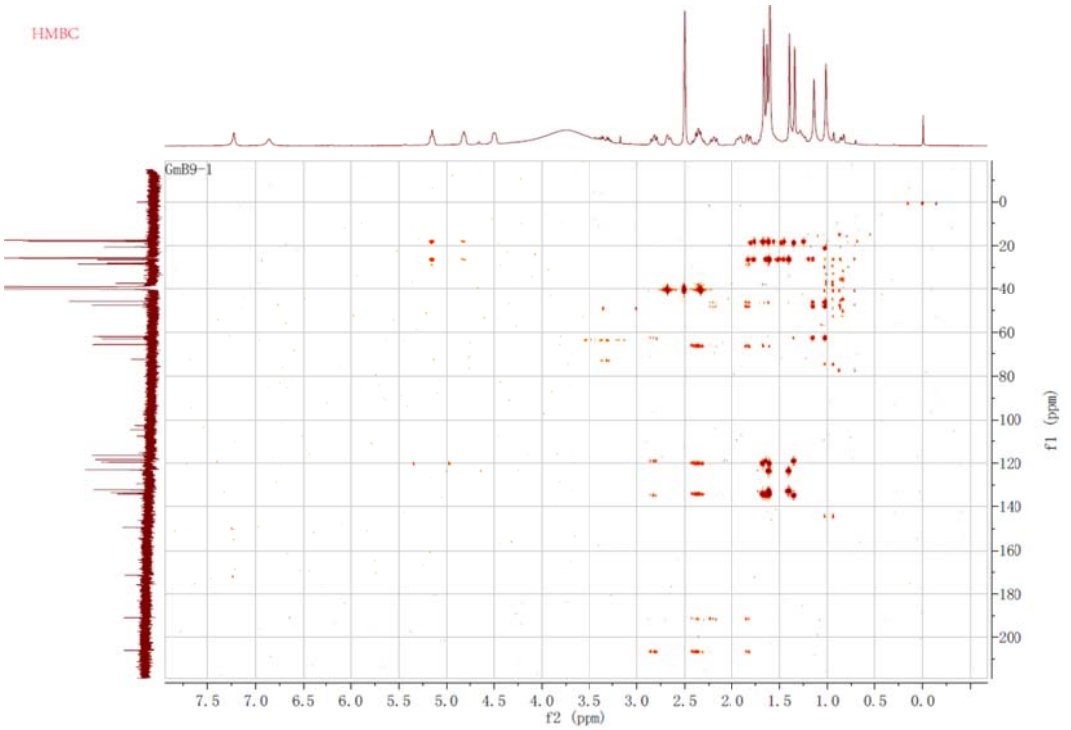

Figure S20. TOCSY NMR spectrum (DMSO-d_6, 600 MHz) of **2**

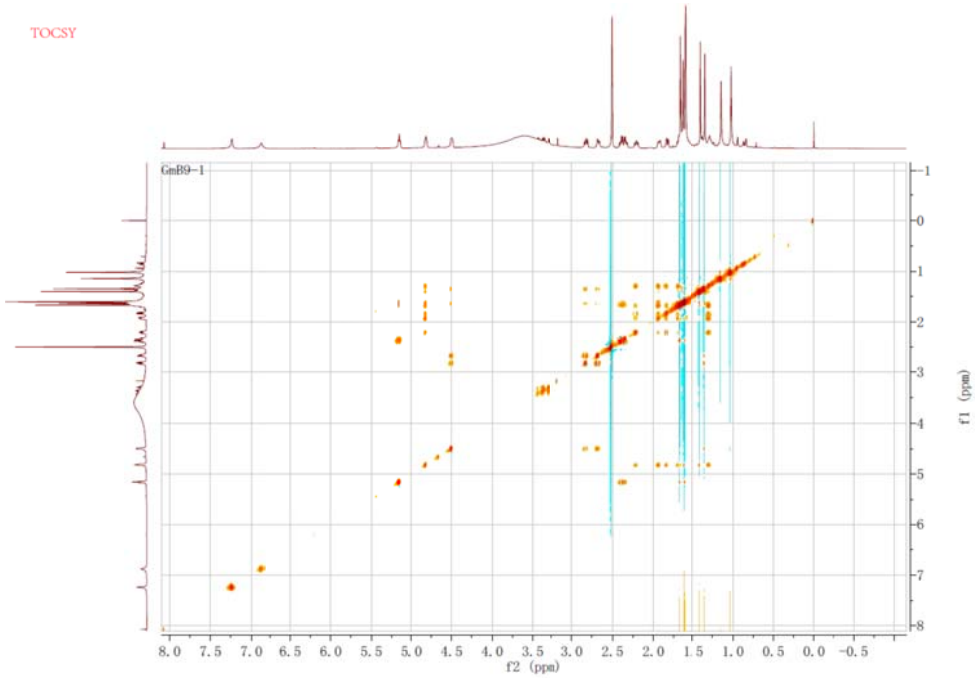

Figure S21. NOSEY NMR spectrum (DMSO-d_6, 600 MH_Z) of **2**

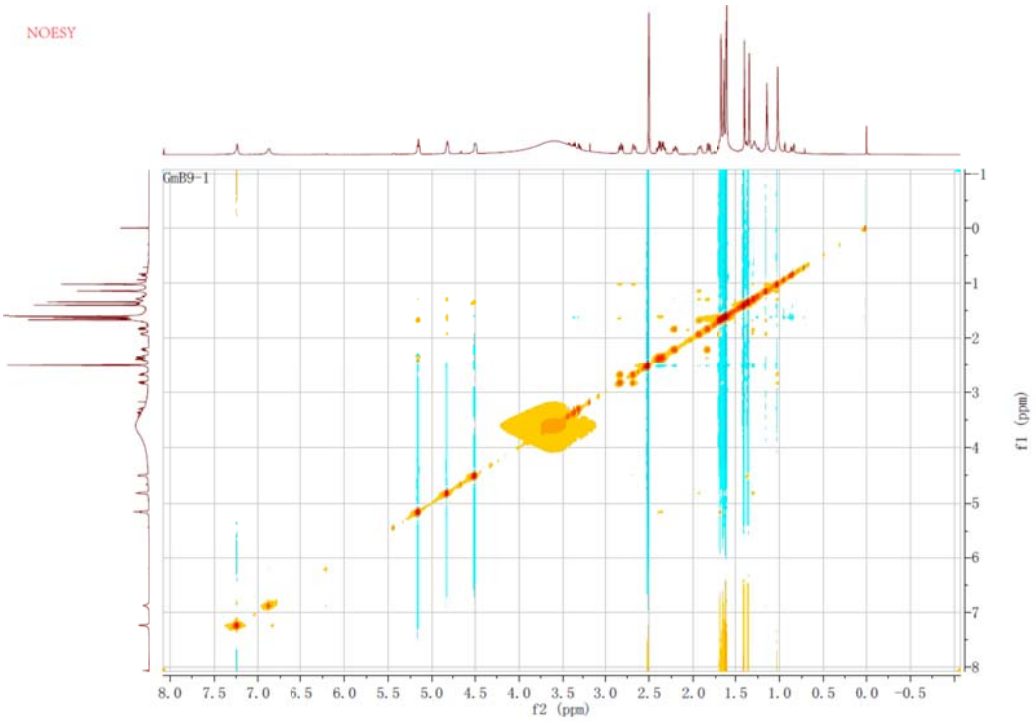

Figure S22. HRESIMS spectrum of **3**

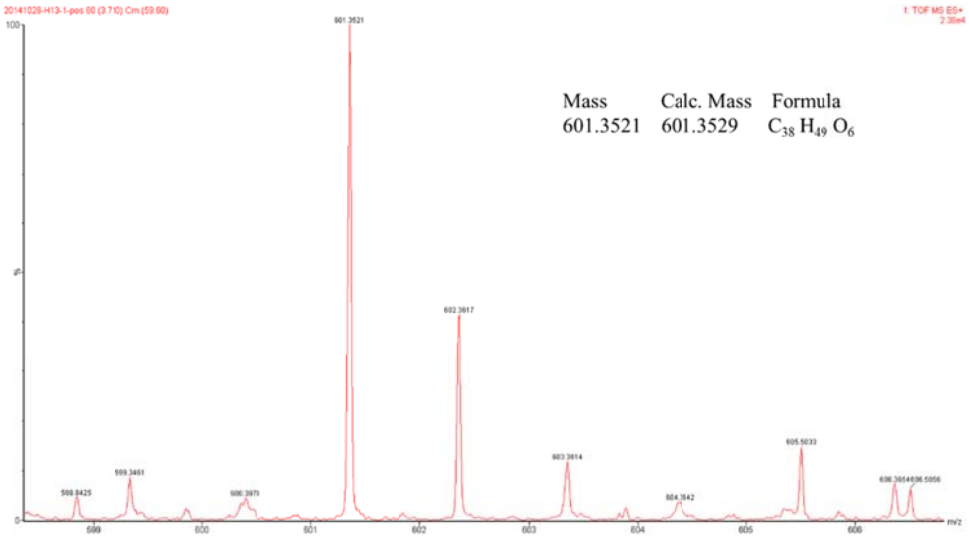

Figure S23. Experimental UV spectrum of **3**

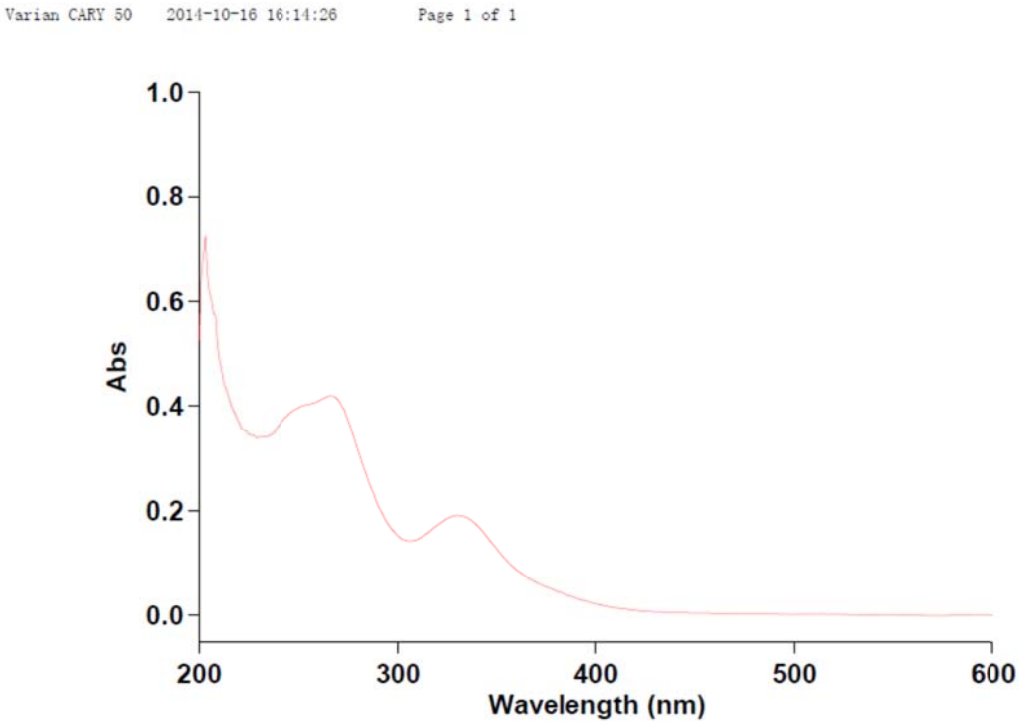

Figure S24. Experimental ECD spectrum of **3**

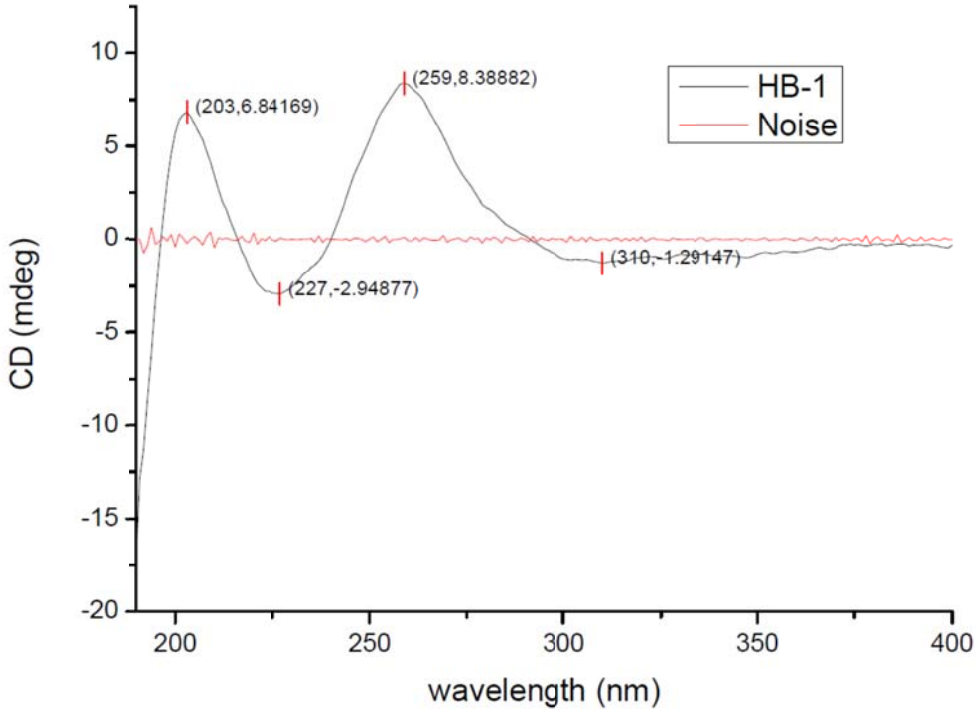

Figure S25. IR (KBr, disc) spectrum of **3**

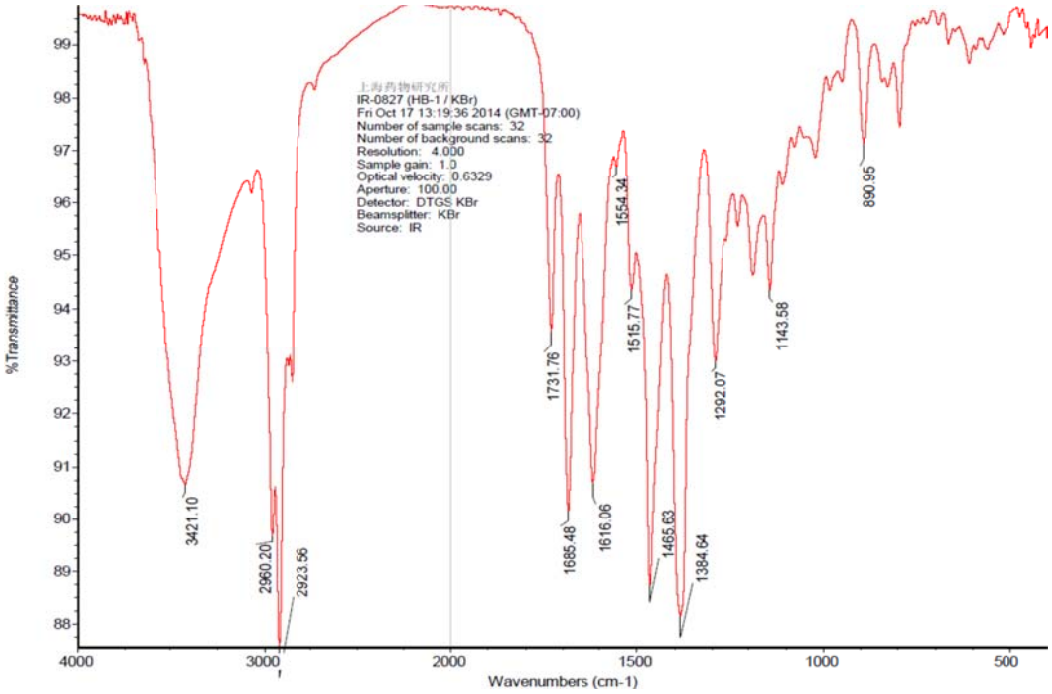

Figure S26. ^{1}H NMR spectrum (CD_3OD, 600 MH_Z) of **3**

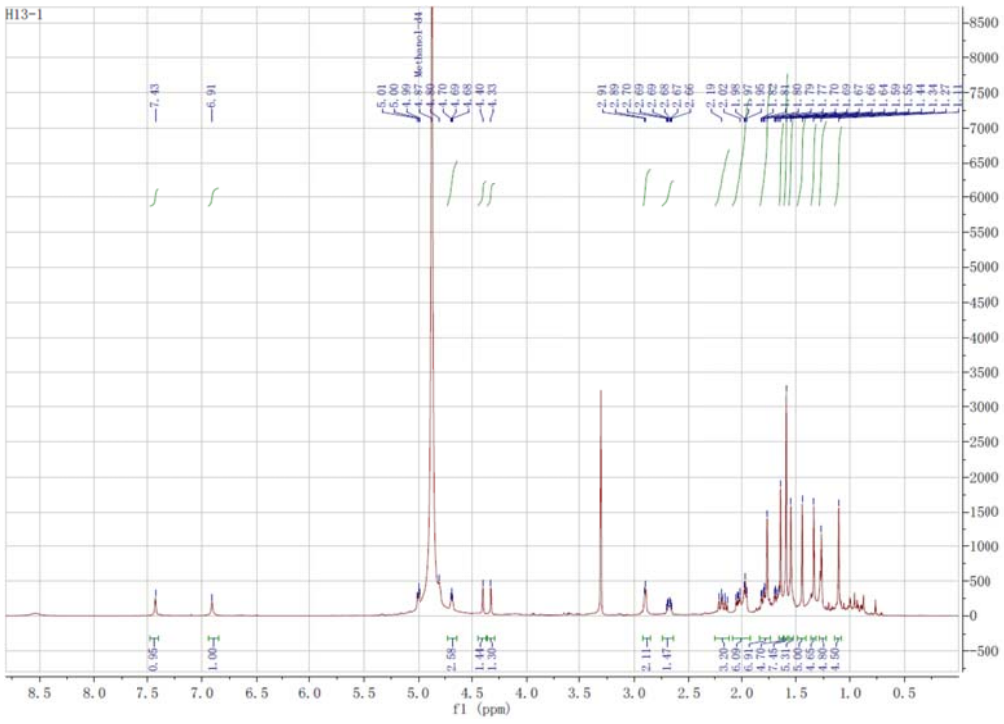

Figure S27. ^{13}C NMR spectrum (CD_3OD, 150 MH_Z) of **3**

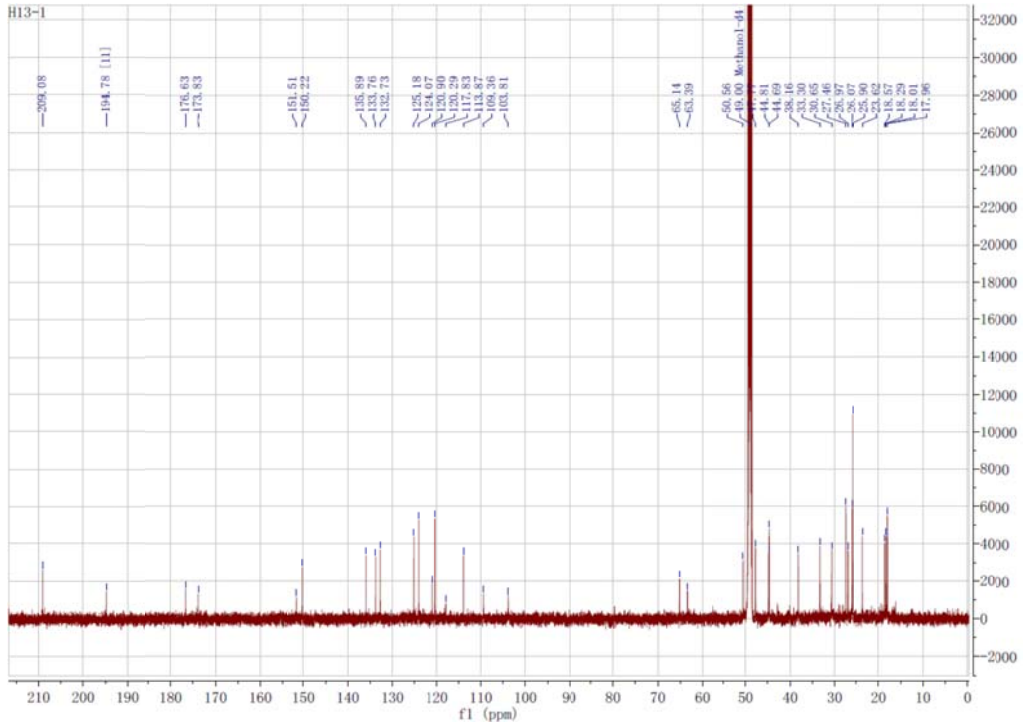

Figure S28. DEPT NMR spectrum (CD_3OD, 150 MH_Z) of **3**

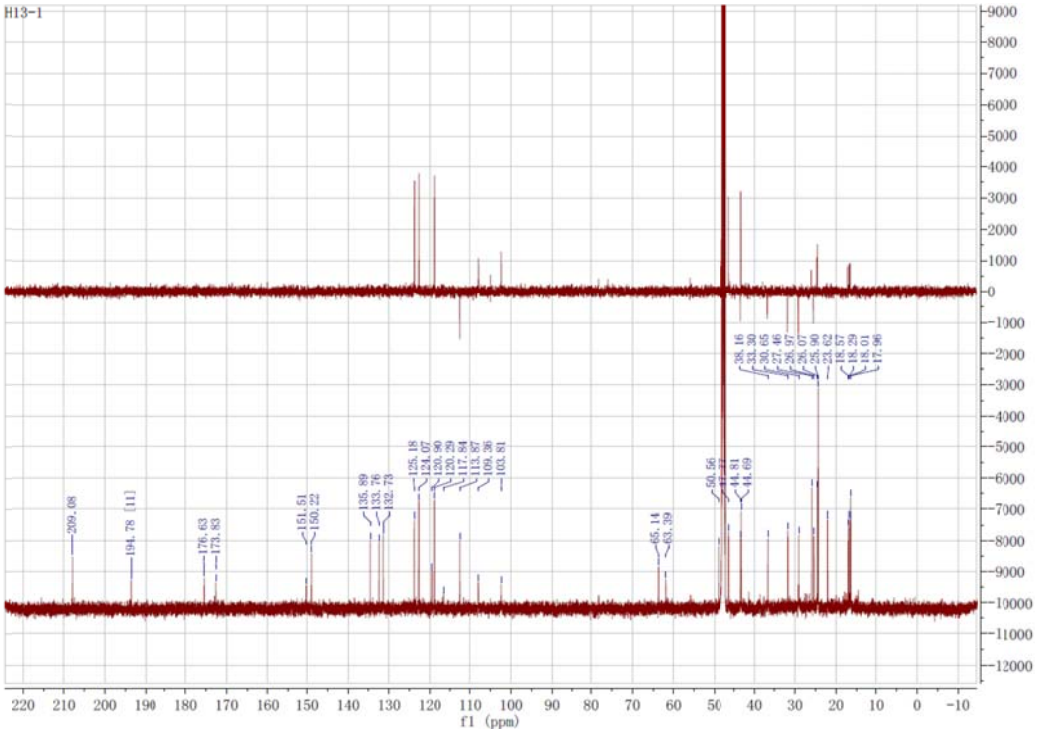

Figure S29. HSQC NMR spectrum (CD_3OD, 600 MH_Z, 150 MH_Z) of **3**

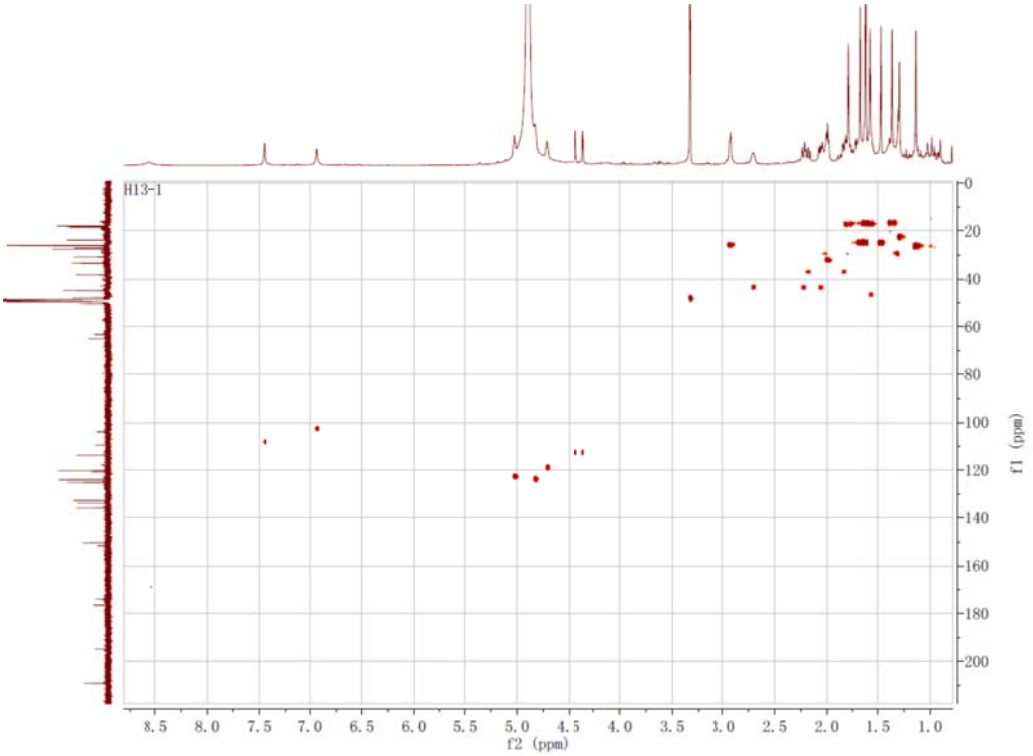

Figure S30. HMBC NMR spectrum (CD_3OD, 600 MH_Z, 150 MH_Z) of **3**

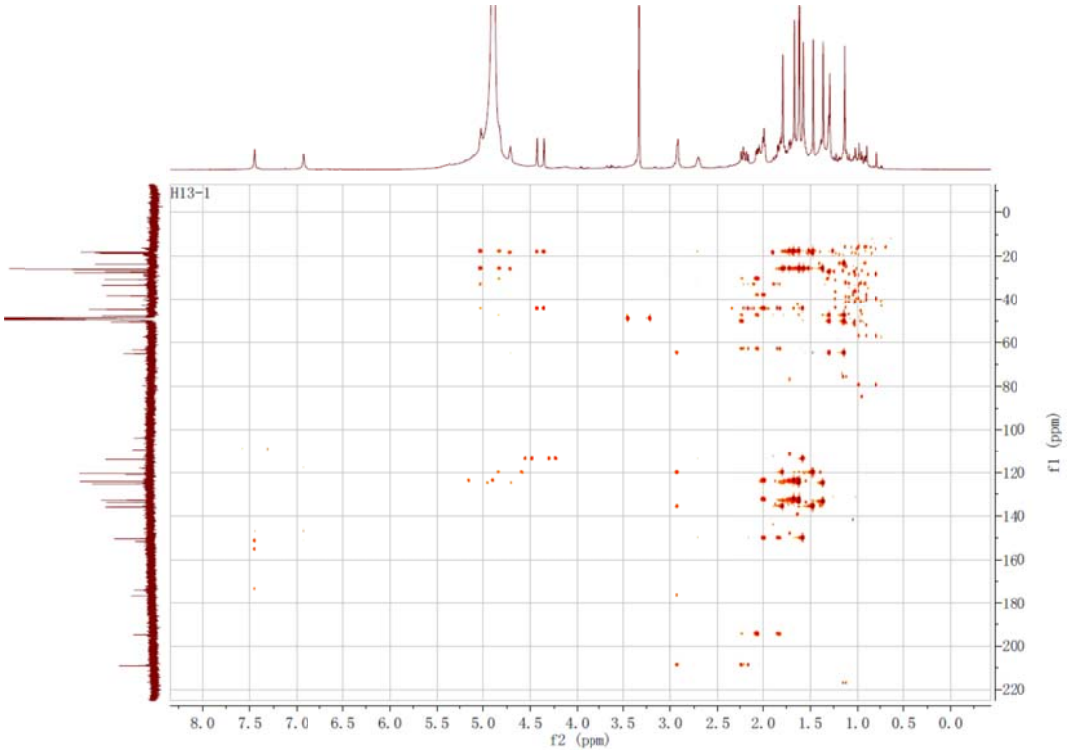

Figure S31. TOCSY NMR spectrum (CD_3OD, 600 MH_Z) of **3**

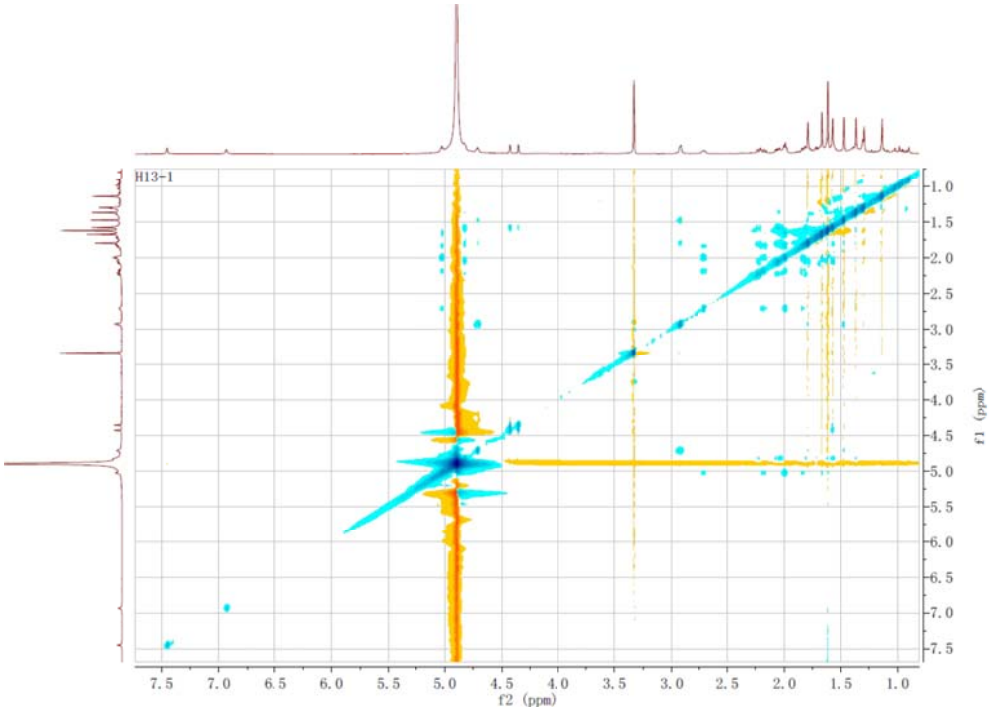

Figure S32. NOSEY NMR spectrum (CD_3OD, 600 MH_Z) of **3**

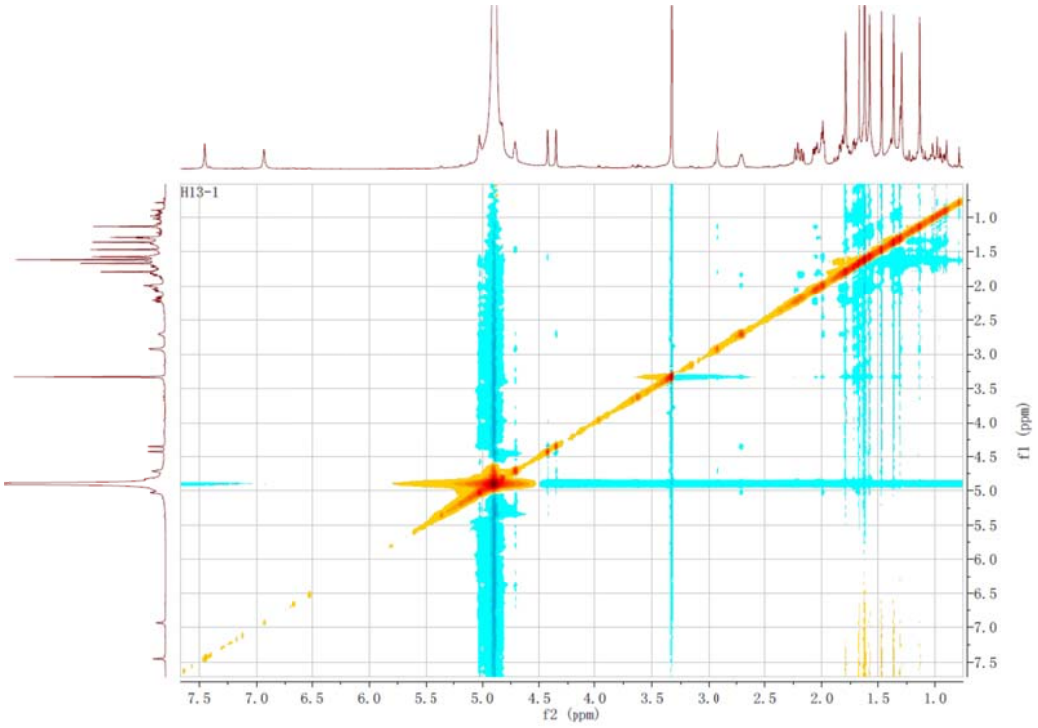

Figure S33. HRESIMS spectrum of **4**

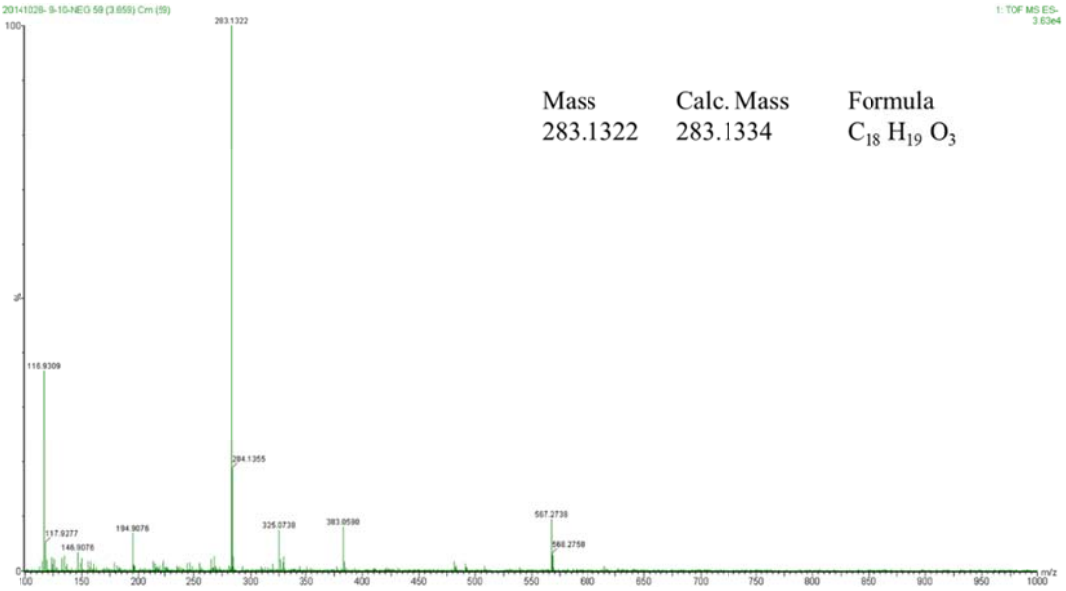

Figure S34. UV spectrum of **4**

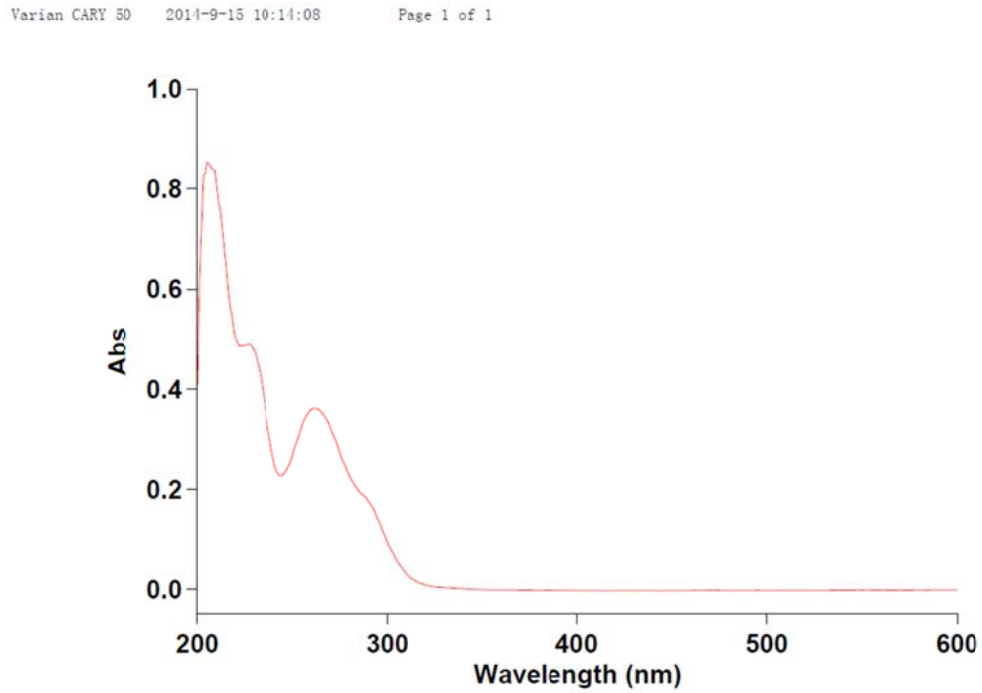

Figure S35. IR (KBr, disc) spectrum of **4**

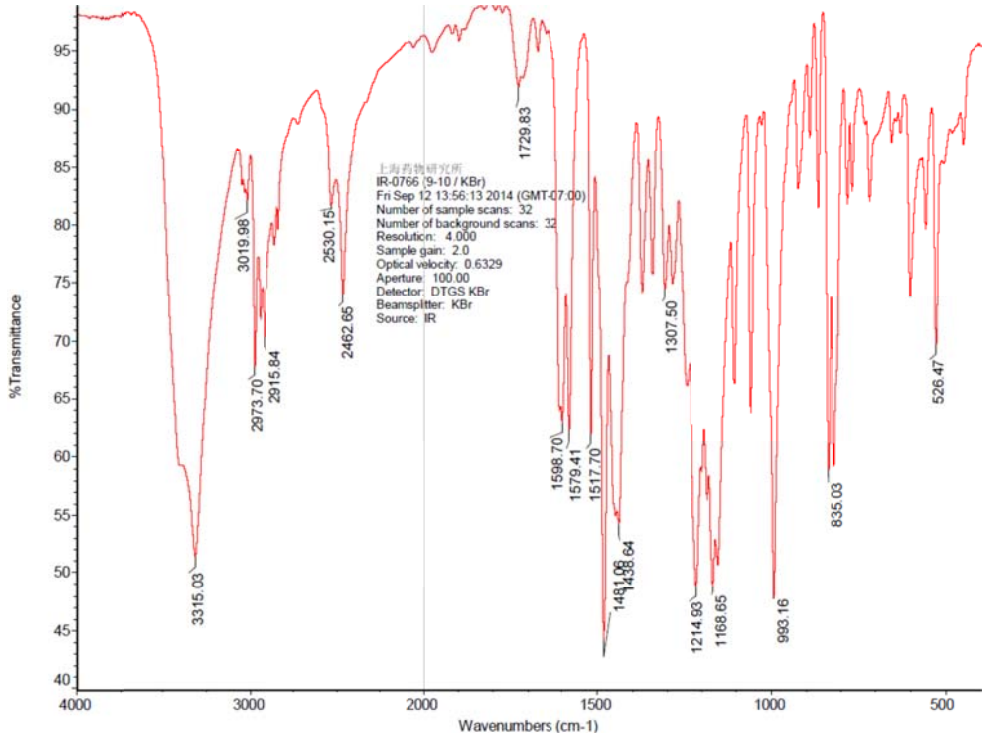

Figure S36. ^{1}H NMR spectrum (CD_3OD, 600 MH_Z) of **4**

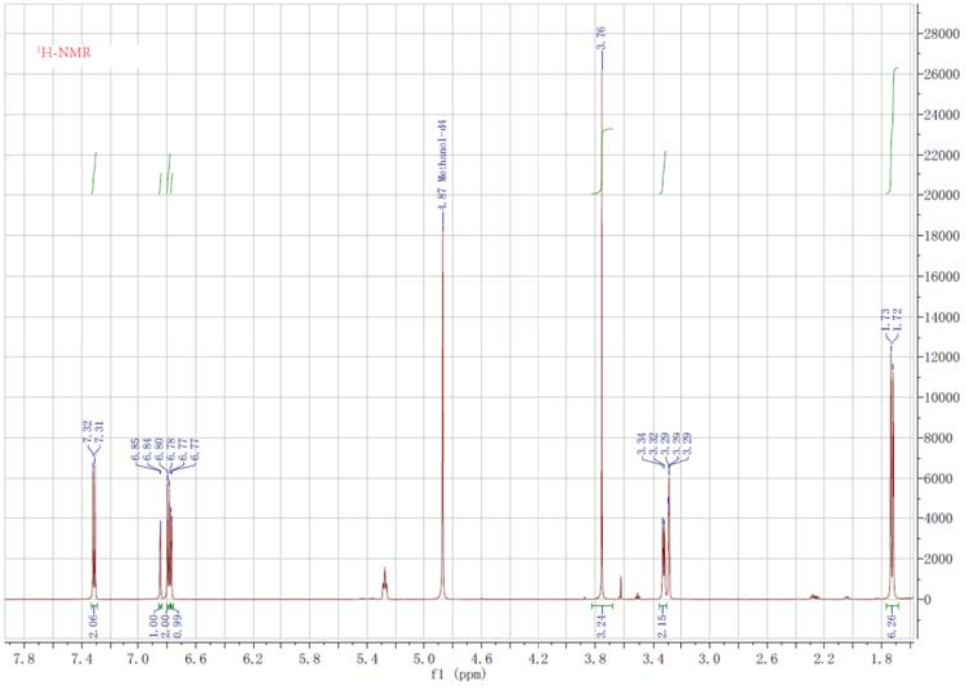

Figure S37. ^{13}C NMR spectrum (CD_3OD, 151 MH_Z) of **4**

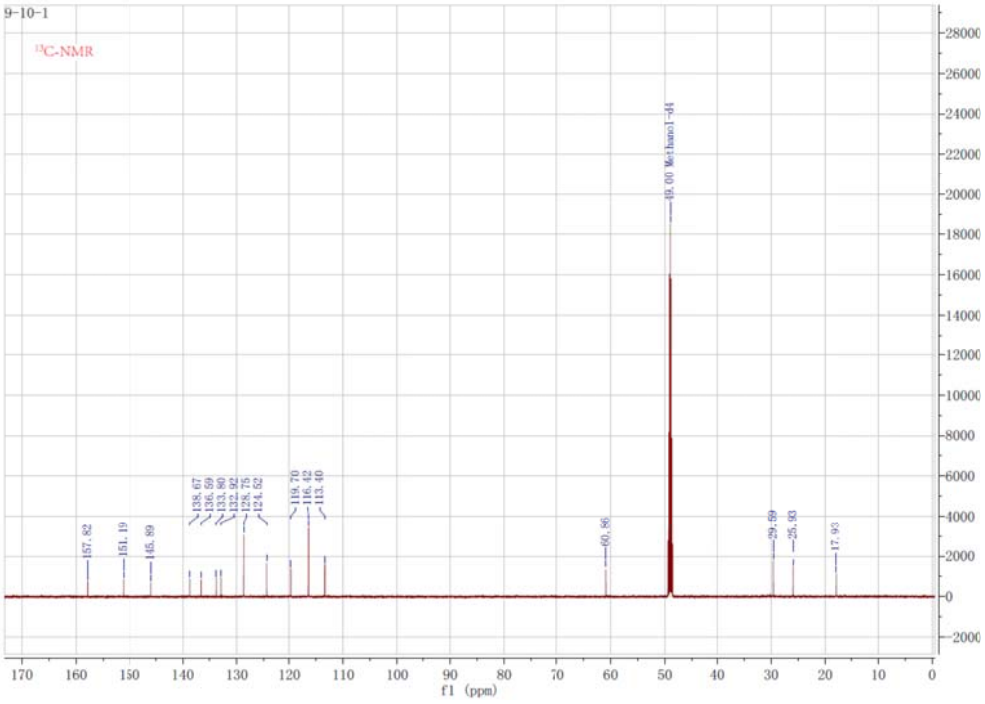

Figure S38. DEPT and ^{13}C NMR spectrum (CD_3OD, 151 MH_Z) of **4**

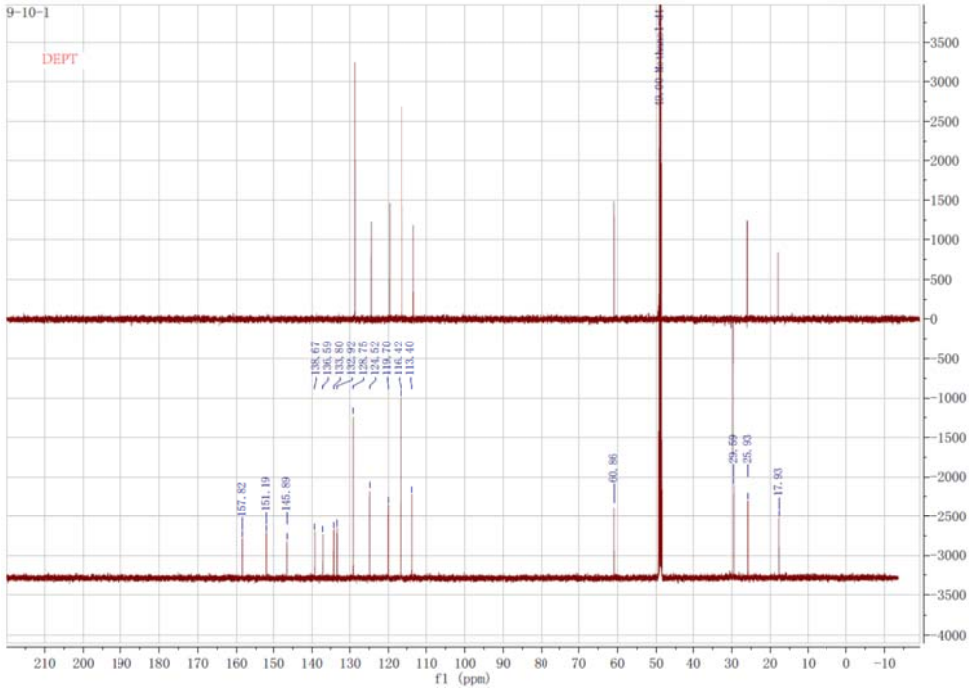

Figure S39. HSQC NMR spectrum (CD_3OD, 600 MH_Z, 151 MH_Z) of **4**

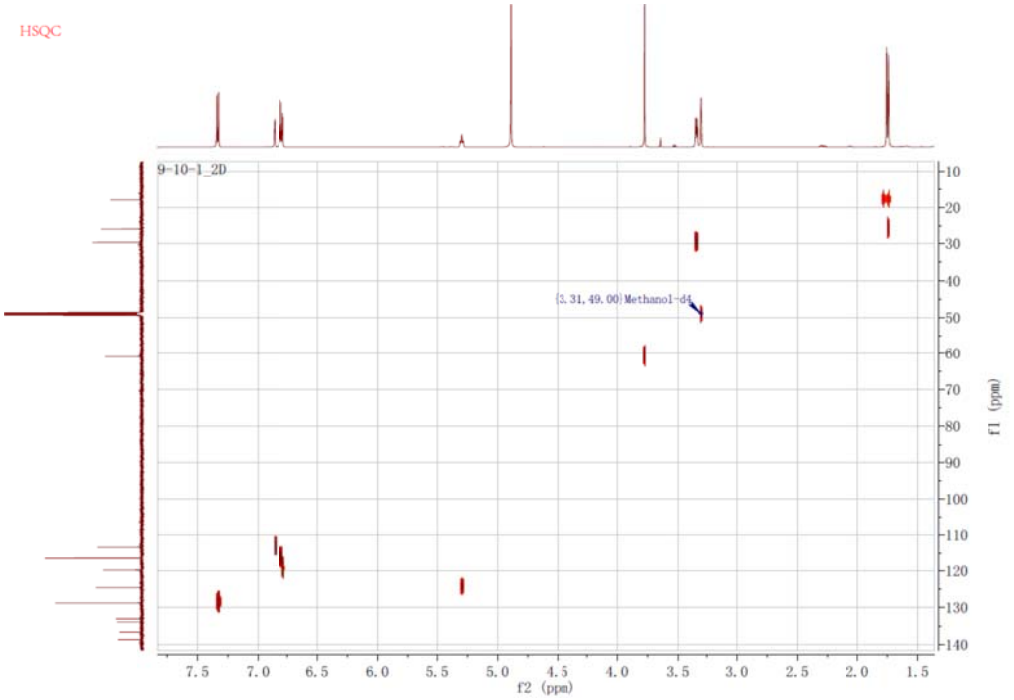

Figure S40. HMBC NMR spectrum (CD_3OD, 600 MH_Z, 151 MH_Z) of **4**

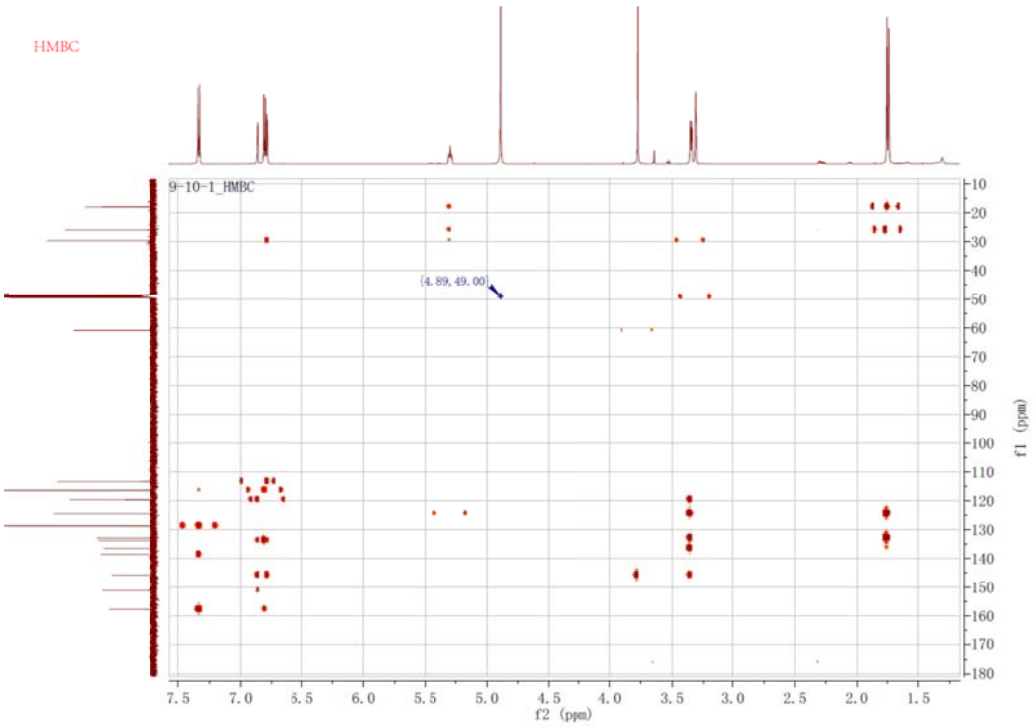

Figure S41. HRESIMS spectrum of **5**

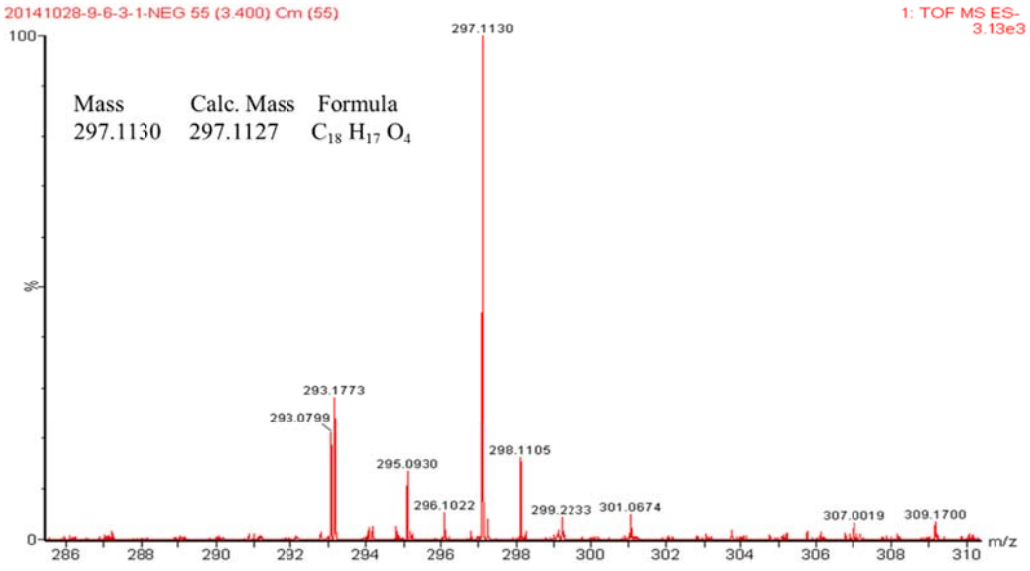

Figure S42. UV spectrum of **5**

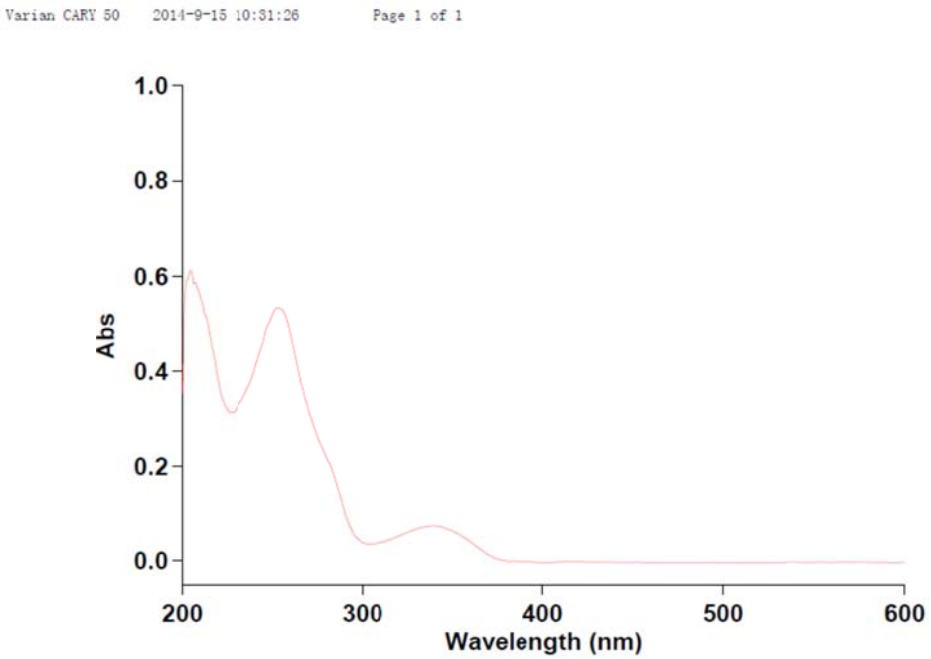

Figure S43. IR (KBr, disc) spectrum of **5**

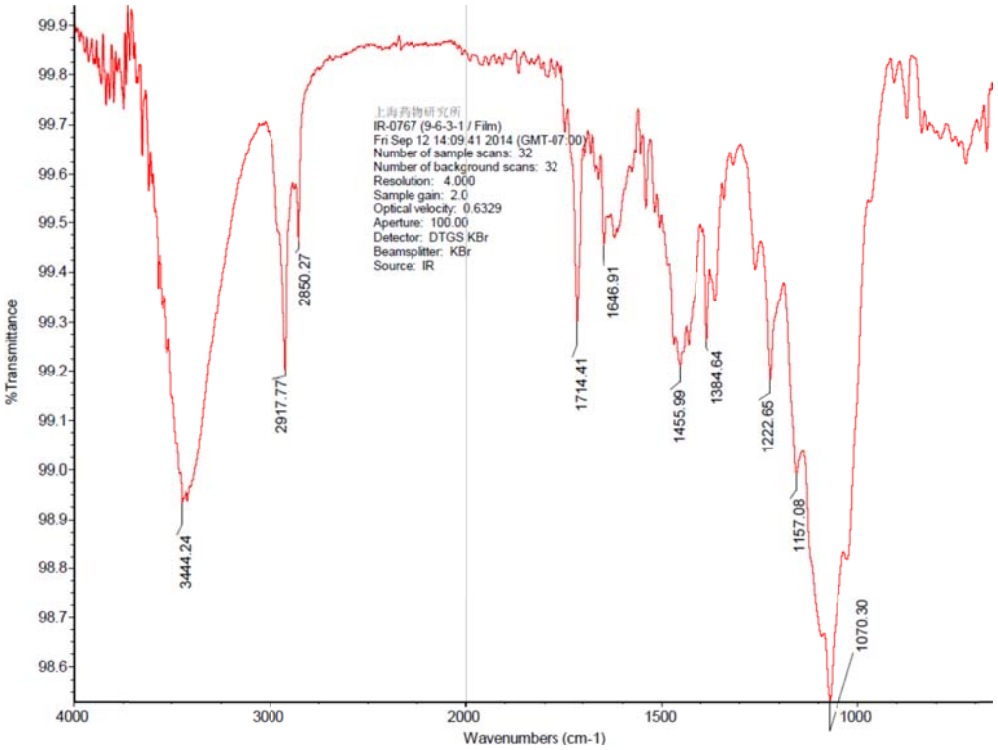

Figure S44. ^{1}H NMR spectrum (DMSO-d_6, 400 MH$_Z$) of **5**

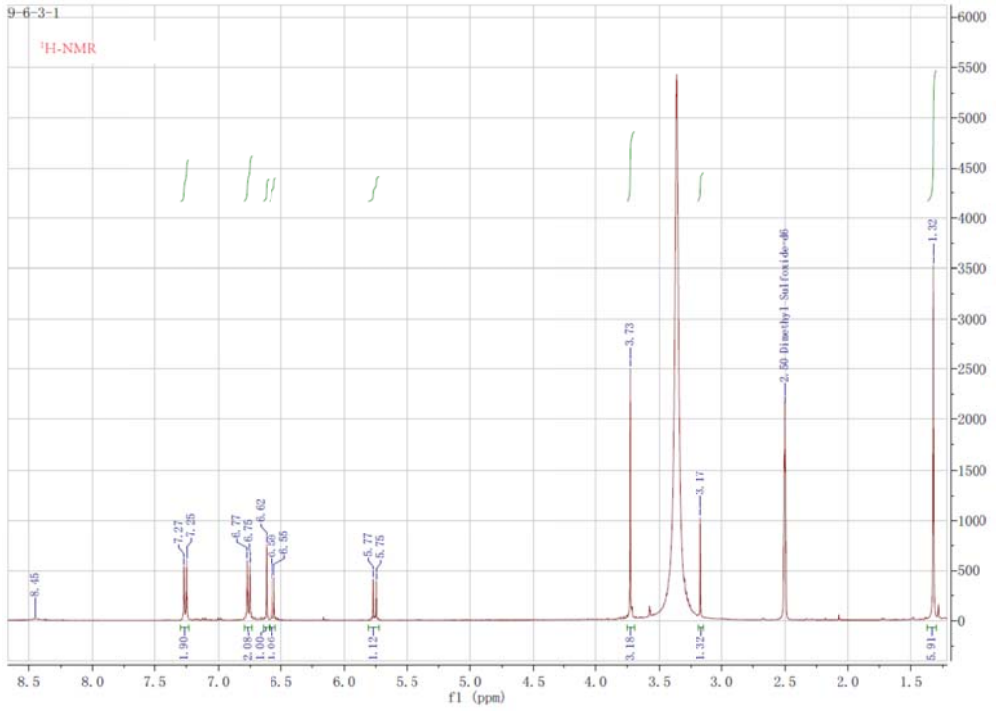

Figure S45. ^{13}C NMR spectrum (DMSO-d_6, 101 MHz) of **5**

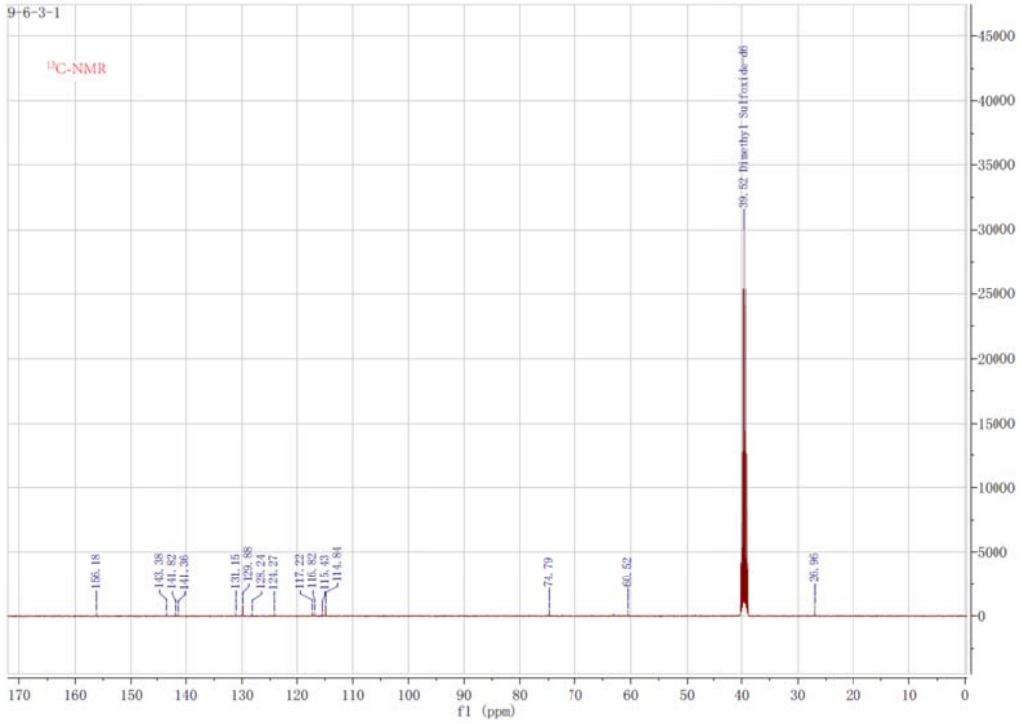

Figure S46. DEPT and ^{13}C NMR spectrum (DMSO-d_6, 101 MHz) of **5**

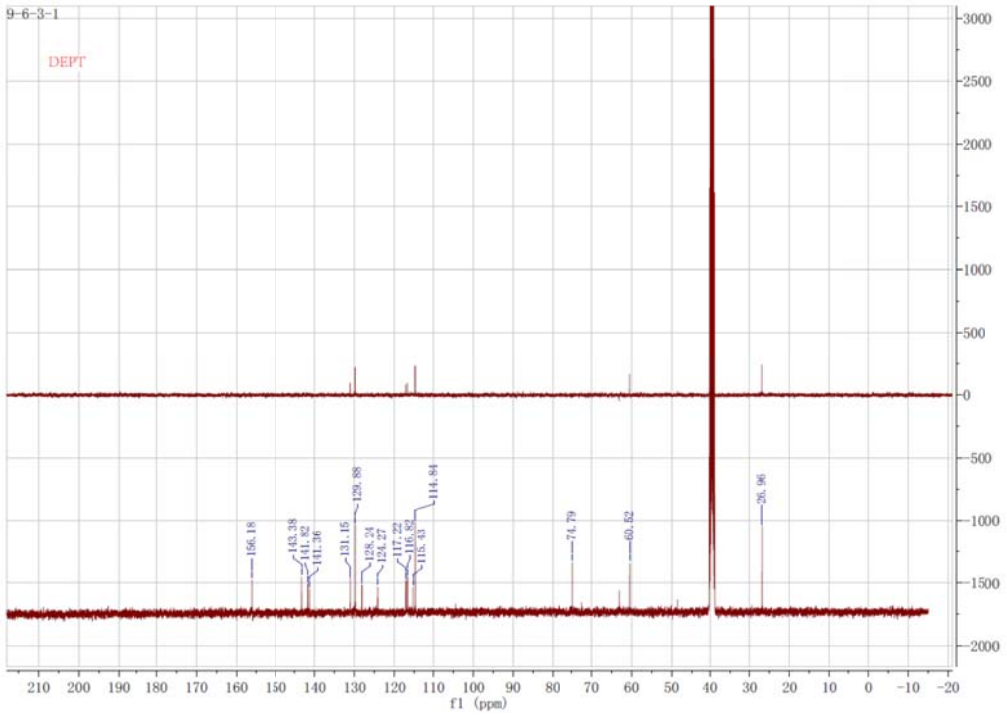

Figure S47. HSQC NMR spectrum (DMSO-d_6, 400 MHz, 101 MHz) of **5**

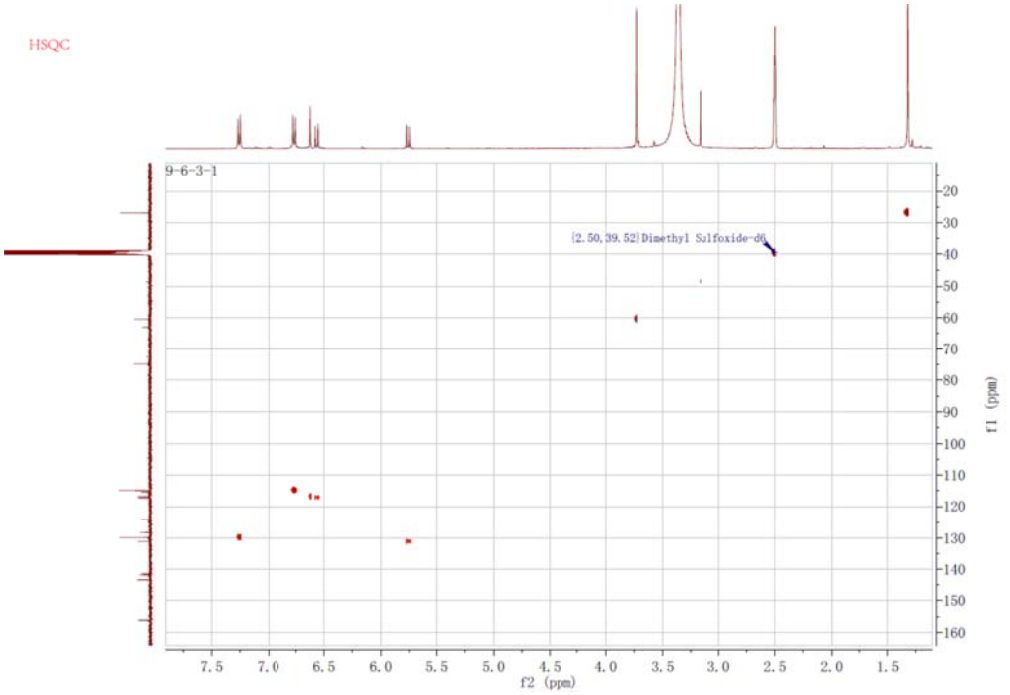

Figure S48. HMBC NMR spectrum (DMSO-d_6, 400 MHz, 101 MHz) of **5**

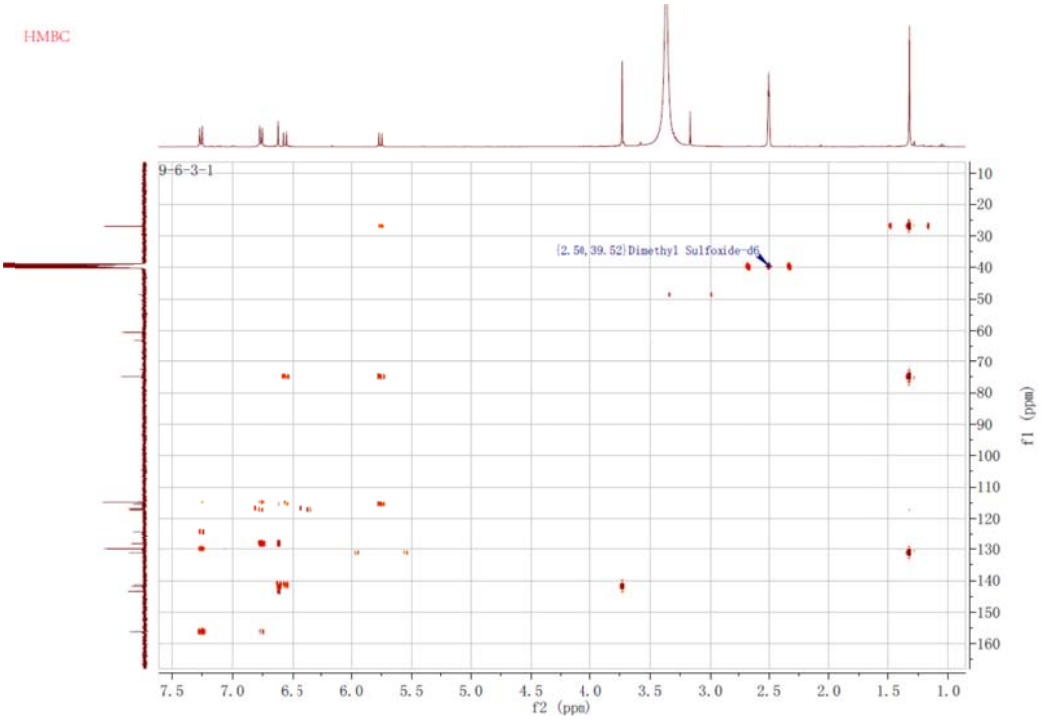

Figure S49. HRESIMS spectrum of **6**

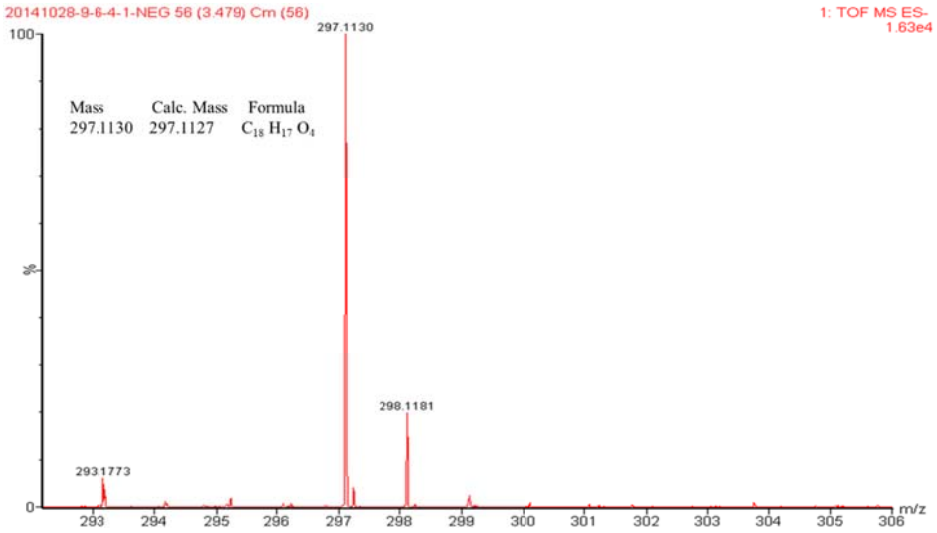

Figure S50. UV spectrum of **5**

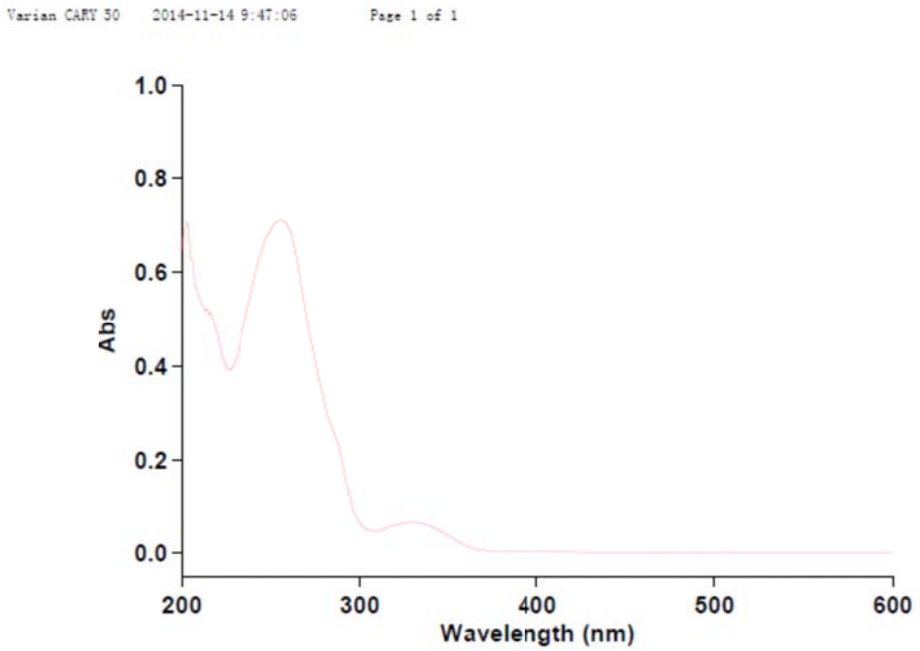

Figure S51. IR (KBr, disc) spectrum of **6**

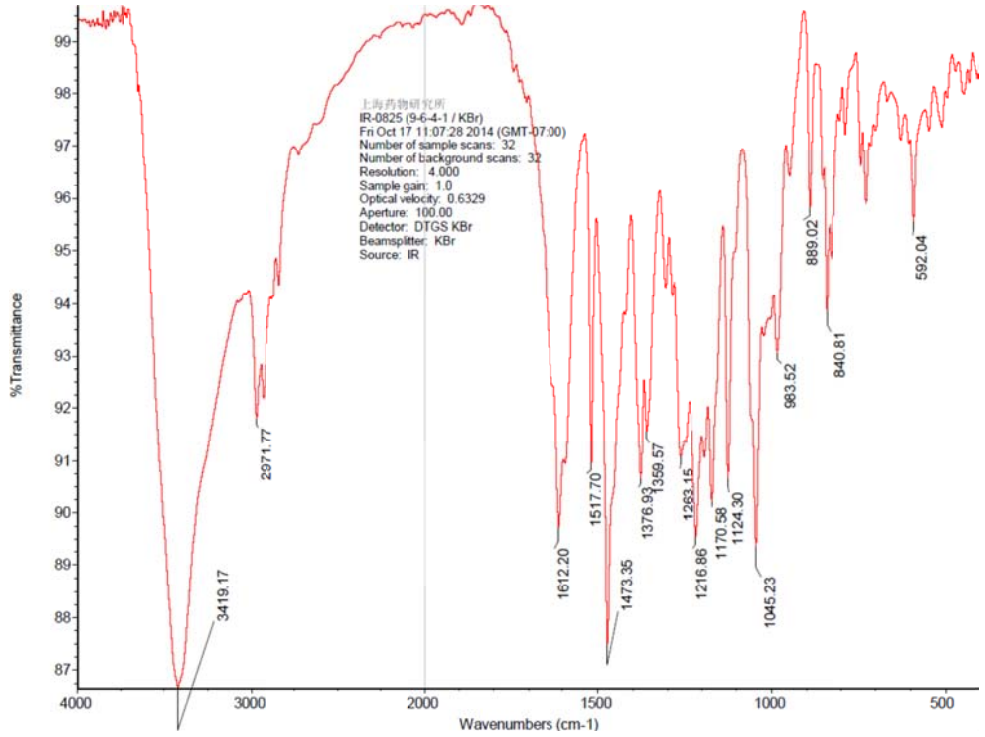

Figure S52. ^{1}H NMR spectrum (CD_3OD, 600 MH_Z) of **6**

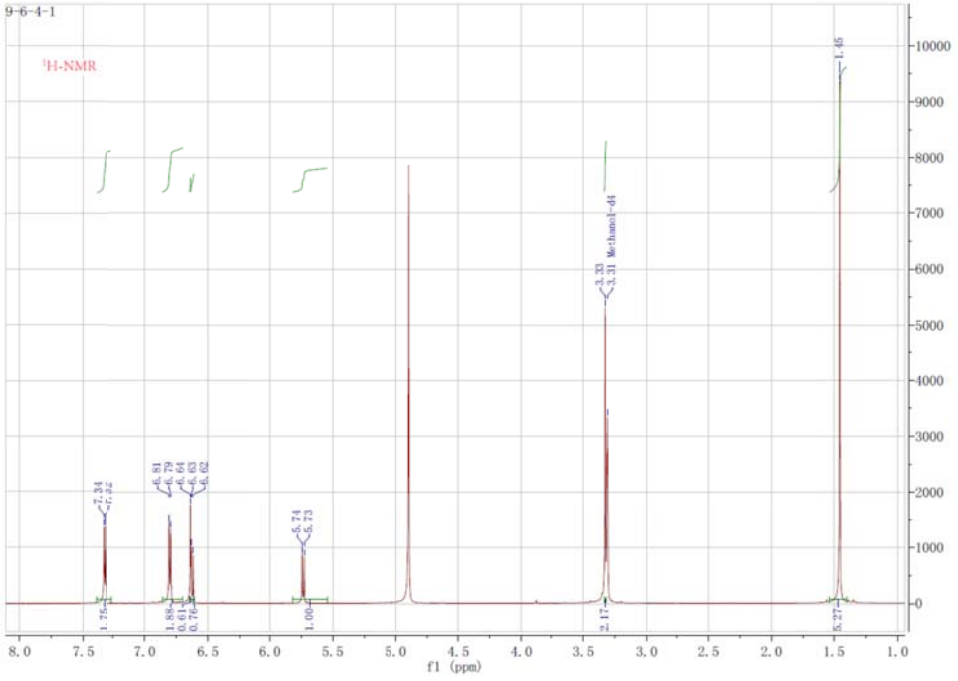

Figure S53. ^{13}C NMR spectrum (CD_3OD, 151 MH_Z) of **6**

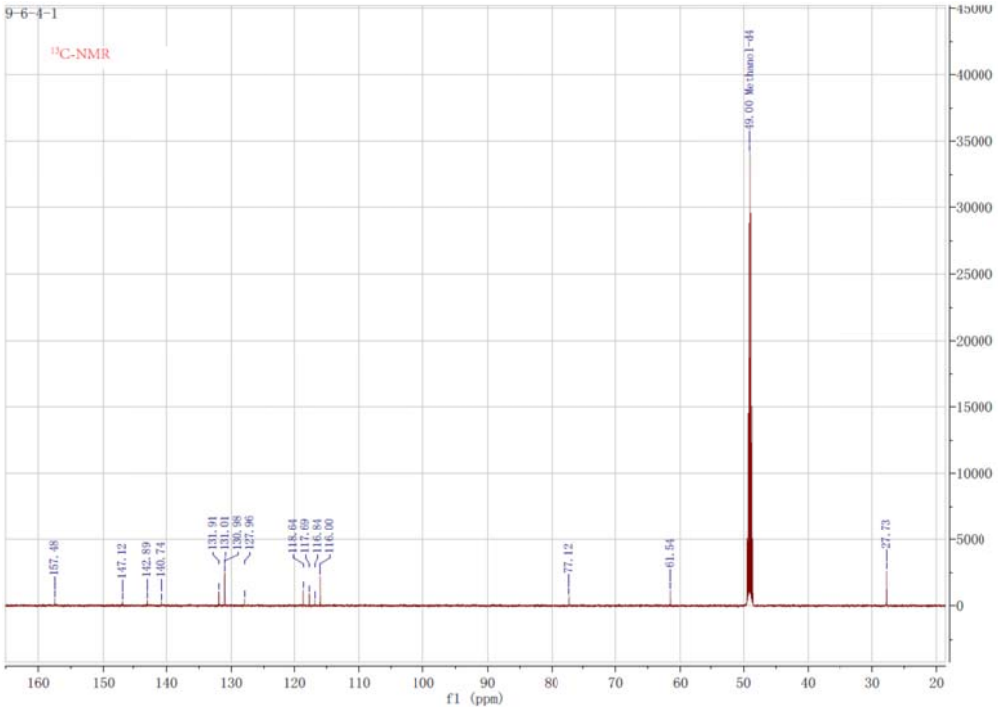

Figure S54. DEPT and ^{13}C NMR spectrum (CD_3OD, 151 MH_Z) of **6**

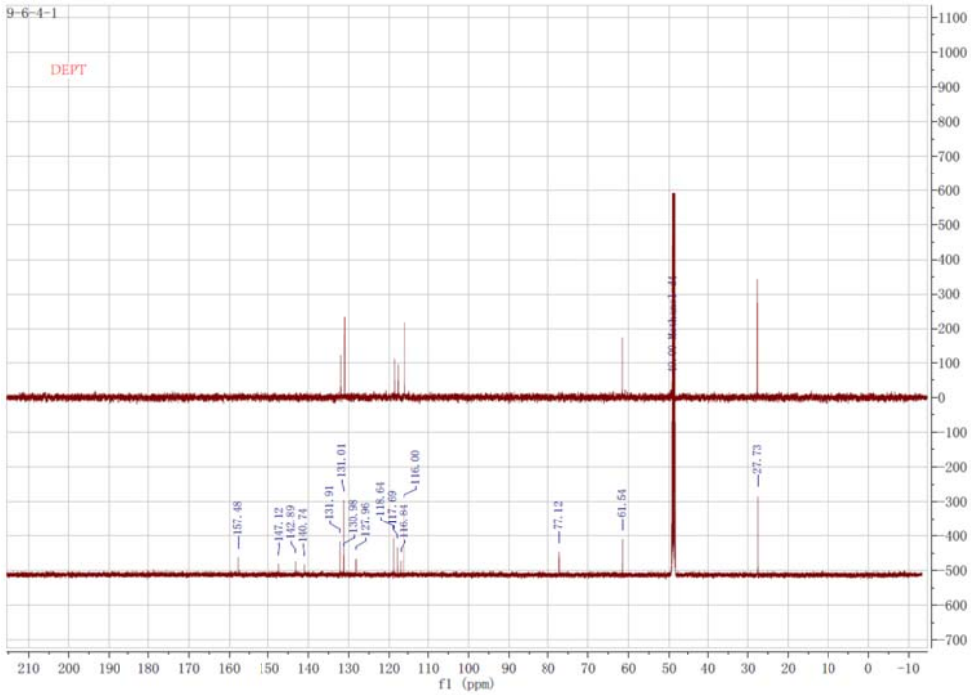

Figure S55. HSQC NMR spectrum (CD_3OD, 600 MH_Z, 151 MH_Z) of **6**

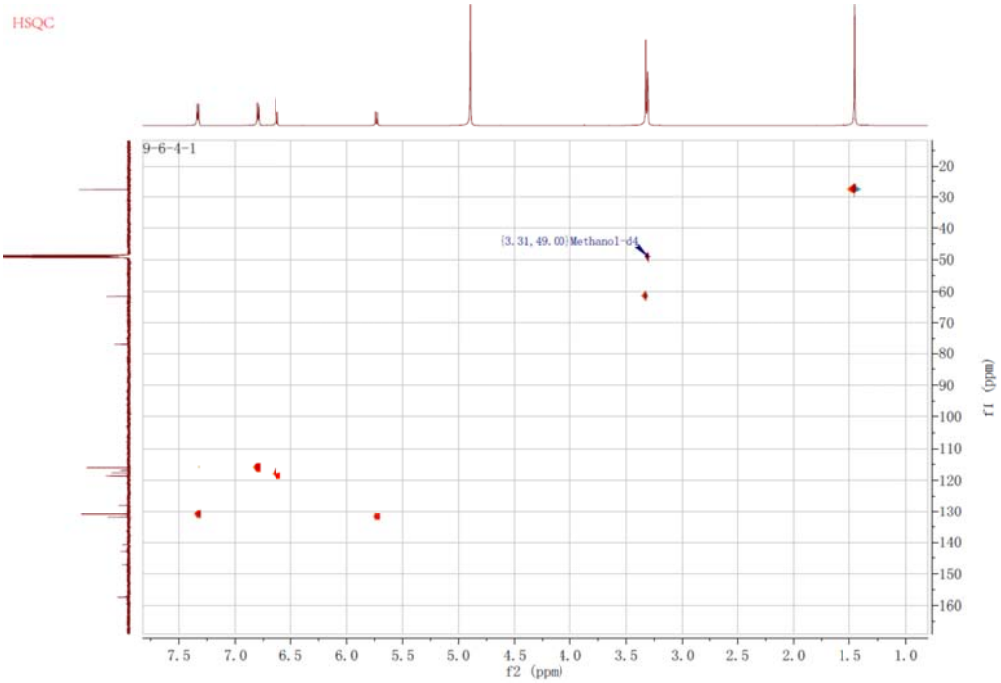

Figure S56. HMBC NMR spectrum (CD_3OD, 600 MH_Z, 151 MH_Z) of **6**

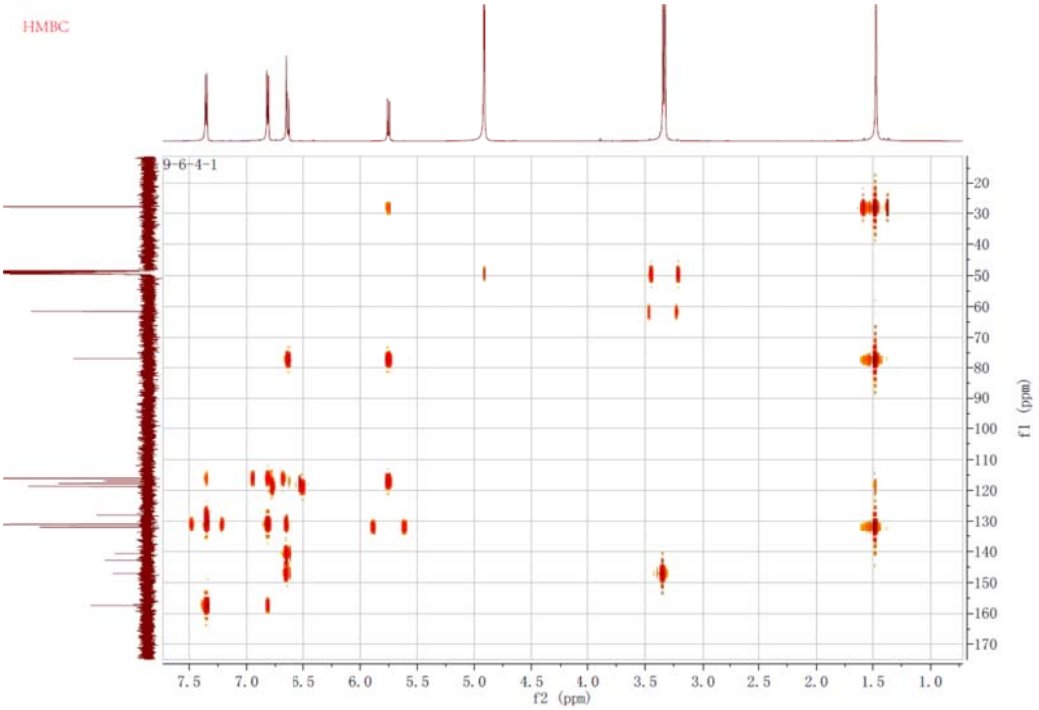

Figure S57. HPLC and LC-MS of GF-ox1

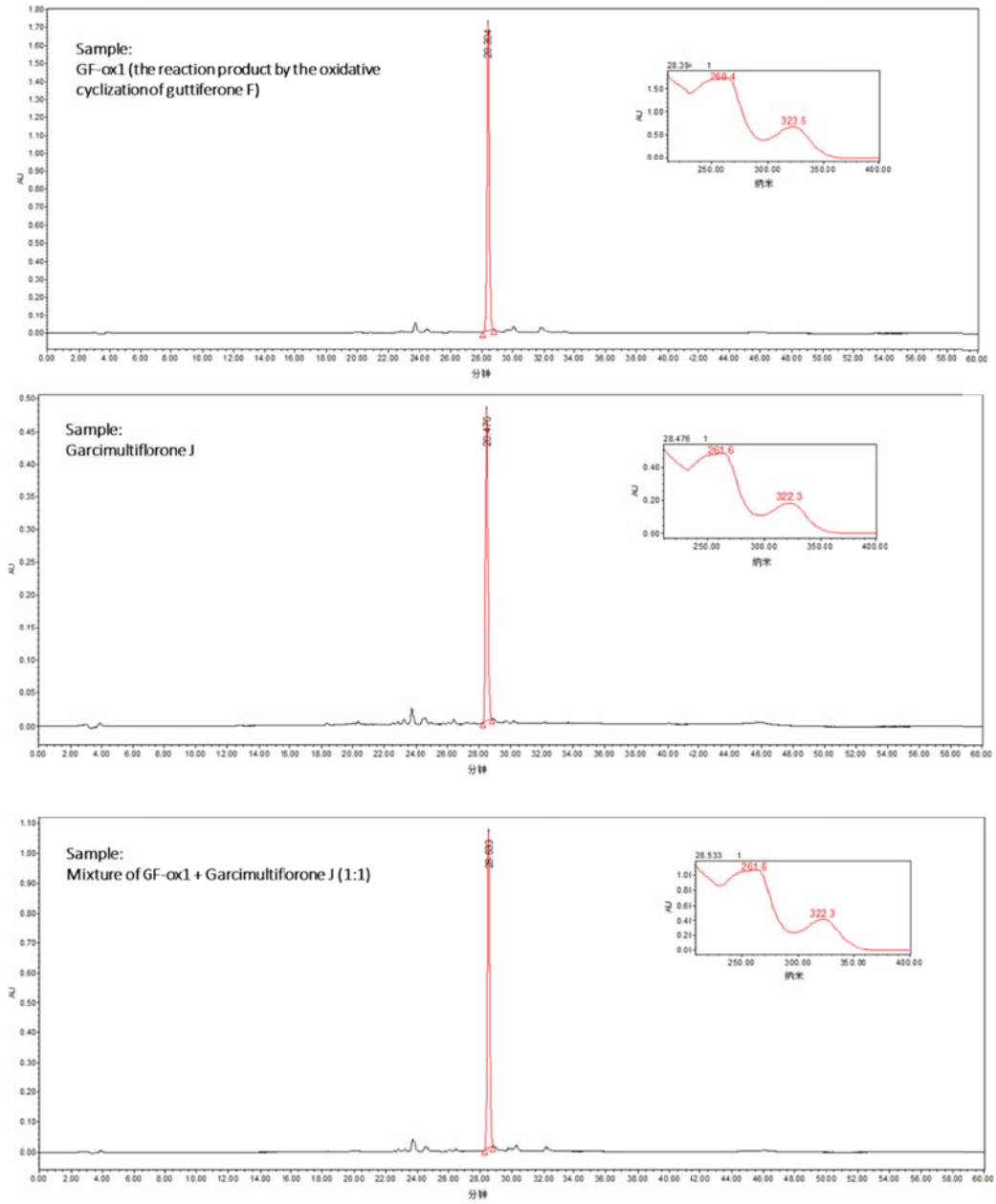

HPLC conditions: All separations were performed on a Shim-pack VP-ODS C18 HPLC Column (4.6 mm × 250 mm, 4.5 μ m, GL/Shimaduz, Japan). The mobile phase consisted of (A) 0.1% formic acid in water and (B) acetonitrile with the following gradient elution: 0–15 min, 30-100% B; 16–35 min, 100% B. The injection volume was 5.0 μL and the flow rate at 1.0 ml/min.

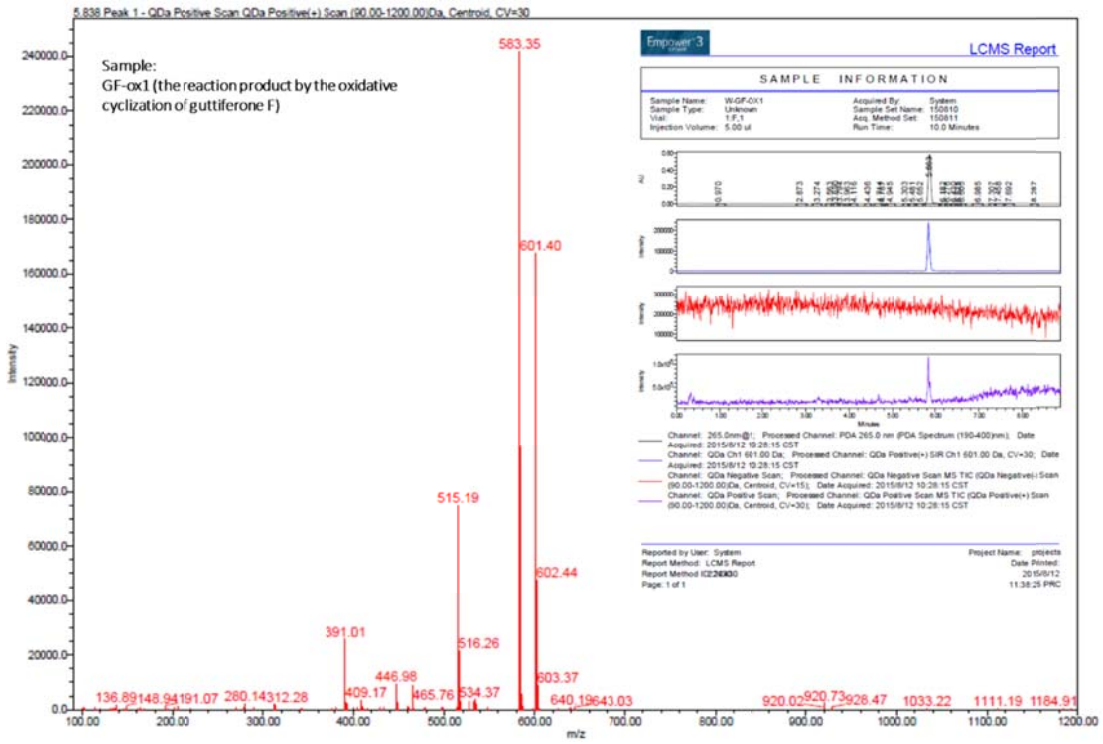

Figure S58. ^{1}H NMR spectrum (CD_3OD, 600 MH_Z) of GF-ox1 and superimposed ^{1}H NMR spectrums

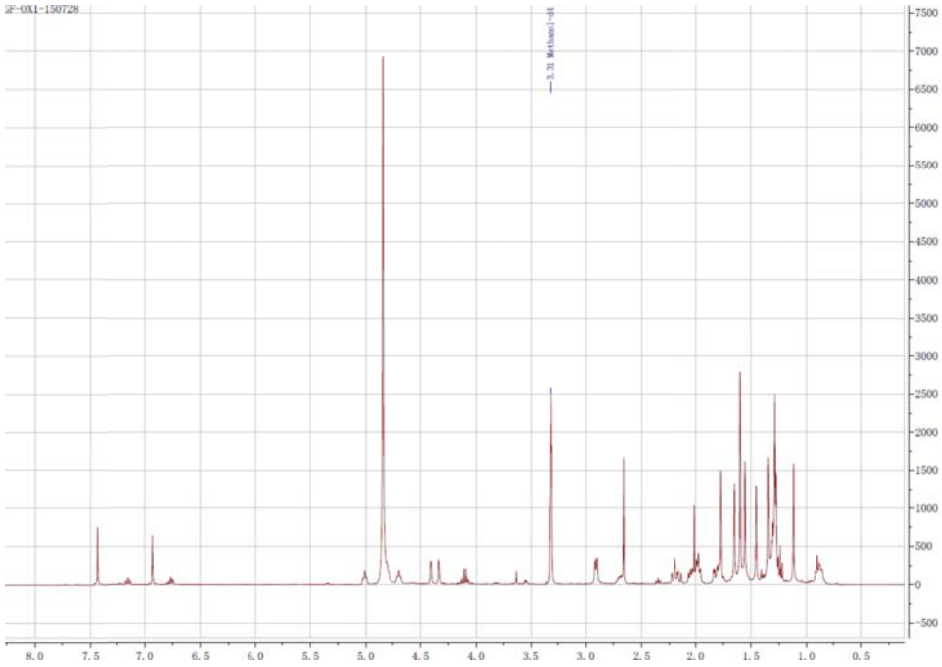

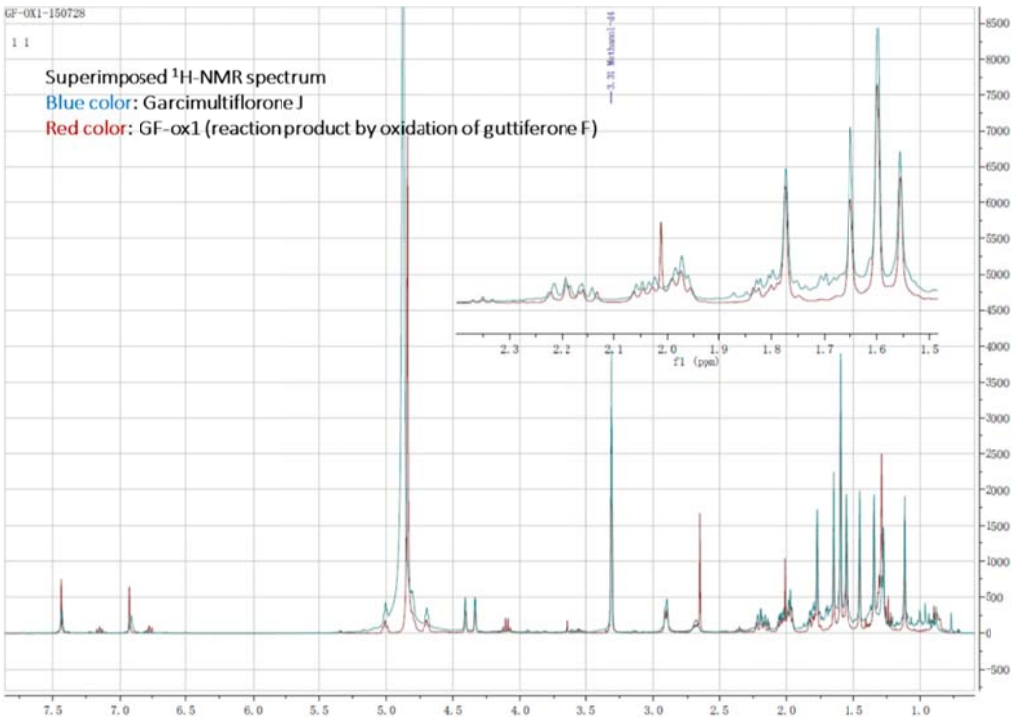

Figure S59. ^{13}C NMR spectrum (CD_3OD, 151 MH_Z) of GF-ox1 and superimposed ^{1}H NMR spectrum of GF-ox1 on Garcimultiflorone J

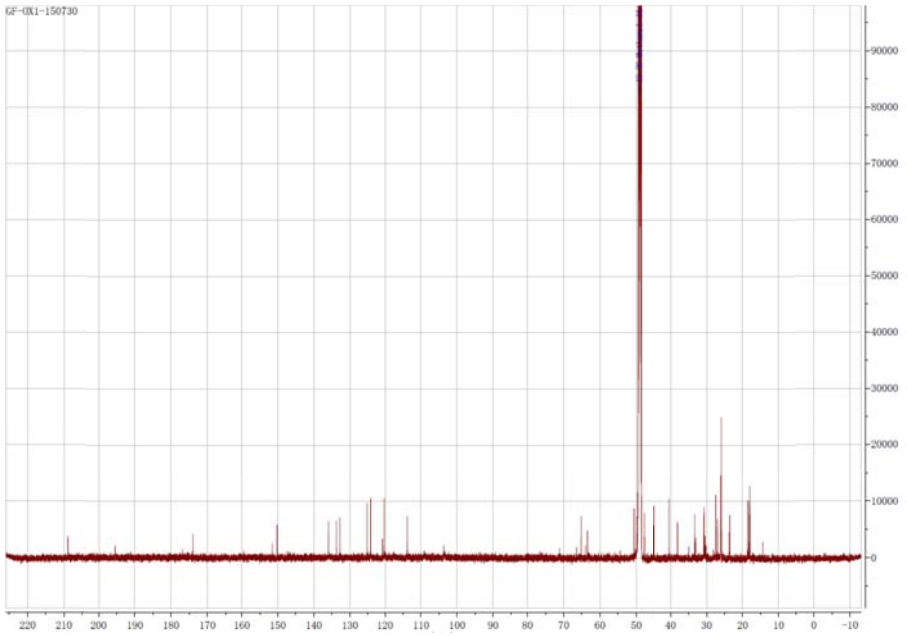

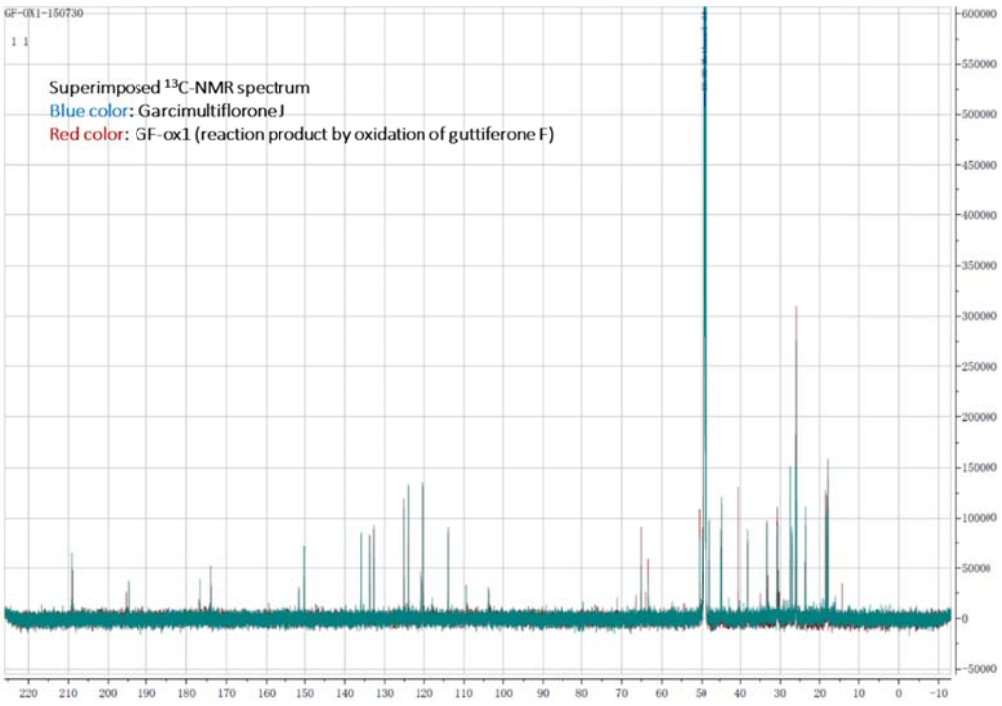

Figure S60. HSQC NMR spectrum (CD_3OD, 600 MH_Z, 151 MH_Z) of of GF-ox1

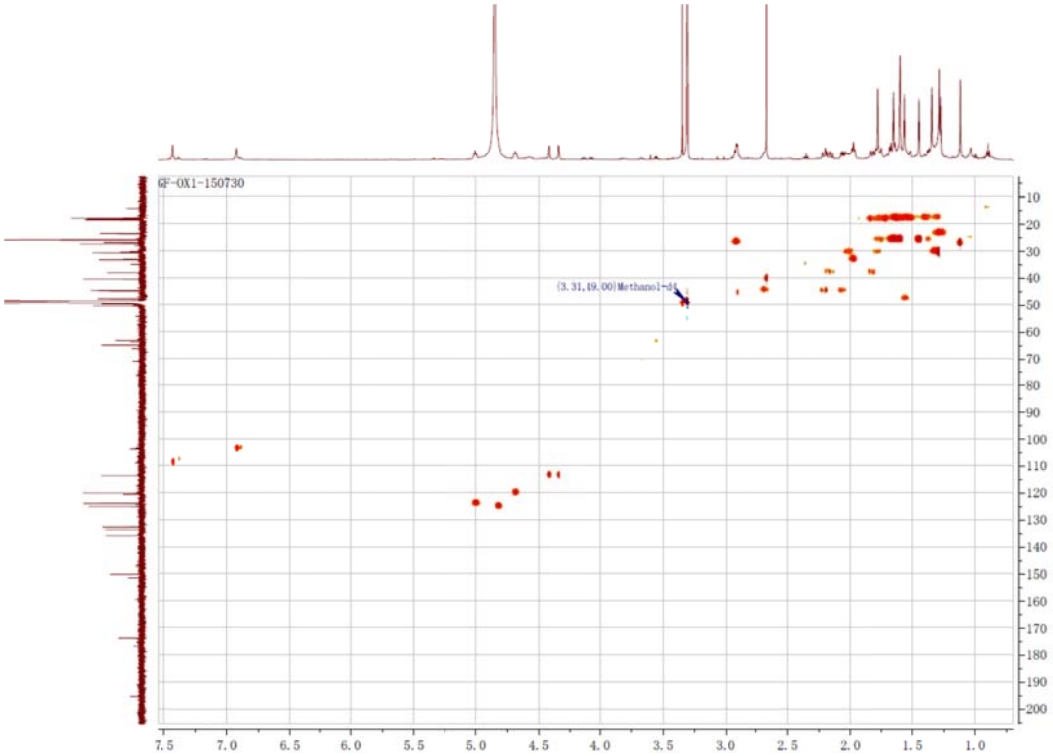

Figure S61. HMBC NMR spectrum (CD_3OD, 600 MH_Z, 150 MH_Z) of GF-ox1